Growth of and Compositional Inhomogeneities in III-V-Bi Alloys

by

Christopher Ryan Tait

A dissertation submitted in partial fulfillment
of the requirements for the degree of
Doctor of Philosophy
(Materials Science and Engineering)
in The University of Michigan
2018

Doctoral Committee:

Professor Joanna Millunchick, Chair
Assistant Professor John Heron
Professor Jamie Phillips
Assistant Professor Liang Qi

Christopher Ryan Tait

rtait@umich.edu

ORCID iD: 0000-0001-5935-9243

Dedication

To my Grandparents, for providing me a path forward in life

Acknowledgments

This work would not have been possible without the countless arguments and support provided by my advisor Joanna Millunchick. The discussions we have contributed to my growth as a person and scientist.

I would like to thank my group mates, Adam Duzik and Matt Dejarld for their mentorship and teaching me the interworking of the lab, and Lifan Yan for her help in material characterization. Professor Chris Pearson was always useful for his experience and willingness to listen to my scientific issues.

Lastly, I would like to thank my wife, Justine Li. Without her, I do not believe I would have started this second endeavor into graduate school. She is always available to make light of the situation and maintain my sanity even with thousands of miles of separation for the last eight years.

Table of Contents

List of Figures

List of Tables

Abstract

Solubility dynamics in materials science drives discovery and novel material development. Bi has garnered interest in III-V semiconductors because of its impact in the electronic properties including large bandgap reduction per percentage Bi, high spin orbit coupling, and preserved electron mobility. The endpoints of III-Bi binary compounds are either unstable, like GaBi, or have low melting point, like InBi. Finding good conditions in which there is appreciable Bi incorporation is difficult. Growths often result in droplets on the surface. This dissertation explores the phenomena surrounding incorporation of Bi including development of computational tools for investigation of Bi impact on electronic structure, a new incorporation model taking Bi surface buildup into account, an investigation into the inhomogeneities that appear along with Ga droplets, and the inhomogeneities that appears in growths with a clean surface. A new kinetic model is constructed to account for Bi buildup on the surface building on previous models. Results of experiments in GaSbBi are utilized to confirm trends predicted in the model. Bi droplets are found to reduce Bi incorporation by becoming a kinetic sink. A series of growths in GaAsBi with varying As:Ga ratio shows that Ga droplets contributes to Bi inhomogeneity in the bulk characterized by x-ray diffraction, transmission electron microscopy, and atom probe tomography. The mechanism associated with this phenomenon is non-uniform Ga availability at the growth surface due to droplet wicking. Growths with clean surfaces are also shown to exhibit inhomogeneities including Bi clusters, lateral composition modulation, and nanopores at growth temperatures below 325°C. These phenomena are explained by a destabilization in the growth mode due to differences in surface diffusivity of As and Bi. Some

preliminary data is presented for future directions including GaAsBi/GaAs superlattices, growth interrupts, and mapping the surface morphology in experiments.

Chapter 1: Introduction

1.1 Introduction

Solubility is a core element of materials science. Manipulating solubility in metallurgy generates routes to novel alloys with a variety of desirable mechanical properties. A good example of this is solubility of carbon in iron. Access to different weight percent of carbon in iron and the phase mixtures associated with it creates the variety of structural properties in steels. In semiconductors, the miscibility of two endpoint compounds determines how easily alloy composition ranges are accessed. For example, InGaAs is calculated to have a miscibility gap with a mixing temperature of ~700K when not under any effects of strain. However when the InGaAs is strained to InAs it is found to have a negative critical temperature indicating it is metastable at all temperatures and compositions[1]. The range of possible compositions in a given semiconductor alloy determines what electronic properties are available such as the band gap. Access to the varied strain states to alter the miscibility is possible with molecular beam epitaxy (MBE) or metal organic chemical vapor deposition (MOCVD).

This dissertation focuses on exploring the mixing behavior of the III-V-Bi alloy systems via MBE. More specifically this work is an investigation of growth conditions for maximal Bi incorporation in III-V semiconductor alloy films while maintaining homogeneous distribution and clean surfaces. The work in this dissertation takes a multifaceted approach to understand the dynamics and impact of Bi incorporation in III-V-Bi alloys. This includes taking steps towards a computational platform for investigating the electronic structure in dilute III-V-Bi alloys,

developing a kinetic model that includes surface buildup of Bi including its impact in Bi incorporation and exploring growth conditions for homogenous Bi distribution in GaAsBi.

1.2 Motivation

Bi containing III-V alloys are of interest due to their potential impact on devices spanning the entire infrared (IR) spectral regime. This spectral range includes materials used in optical communications, night vision, and explosives detection. Many devices in these operating wavelengths experience inefficiencies due to recombination losses and high temperature dependence of the bandgap[2].

Bi is the largest of the group V elements and as such is the final frontier for III-V semiconductor alloys. Based on its position in the periodic table the bonding energy is expected to be low relative to other group V elements. This is reflected in the fact that GaBi is not a stable binary compound and InBi is metallic with a low melting point of 109.5°C[8]. Bi remains an interesting alloying component in III-V materials because of the unique characteristics it exhibits. The potential band gap range of GaAsBi with a bandgap v. lattice constant graph found in Fig. 1-1. The endpoint for GaBi is estimated through density functional theory calculations. It follows and has been shown with the introduction of Bi that it greatly reduces bandgap[2,9–13]. Bi is expected to interact with the band structure through a valence band anticrossing which minimally affects electron mobility [14,15]and consequently been shown that Bi incorporation maintains the electron mobility [13,16].

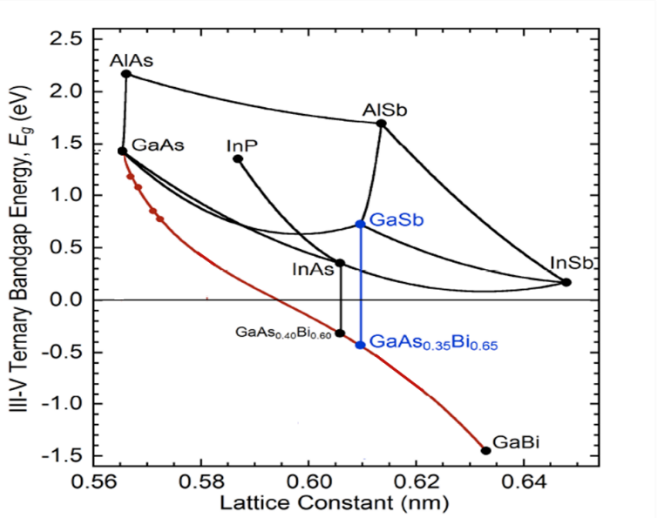

Figure 1-1: III-V ternary alloy bandgap vs. lattice constant diagram including GaBi and estimated GaAsBi bowing curve with lattice matched compositions for InAs and GaSb.

Bi incorporation in GaAs has also been shown to exhibit a large spin orbit coupling increase per percentage Bi[17]. The large spin orbit contribution is due to the size of the Bi atom and enables pathways to minimize Auger recombination losses in devices used in optical communications and IR detection. It could be possible for GaAsBi-based materials to exhibit large enough spin orbit coupling to alleviate conduction-hole spin-hole (CHSH) type Auger recombination, which normally increases the turn-on voltage of lasers in the optical communications wavelength as seen in Fig. 1-2. Electronic characterization of the materials has also occurred resulting in observation of the properties mentioned above including mobility measurements[13,16], temperature and intensity dependent photoluminescence (PL)[11,18,19], and spin orbit lifetime measurements[20].

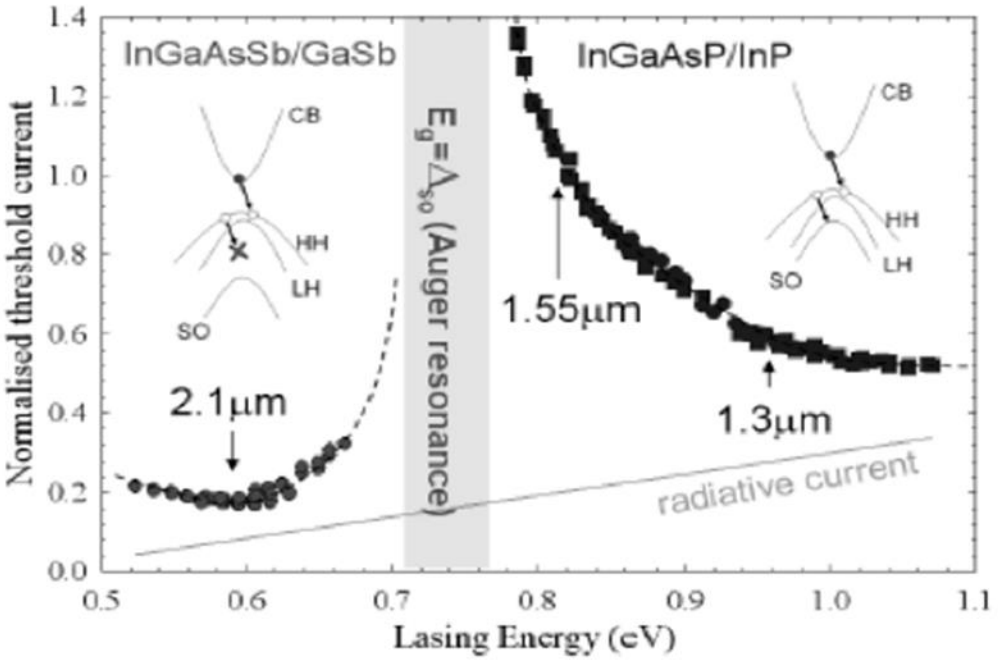

Figure 1-2: Threshold current as a function of lasing energy showing the effect of Auger recombination on infrared devices, the inset illustrates the suppression of CHSH Auger recombination.[2]

For Bi materials to make in impact on IR detector materials it must perform on similar or higher levels to the current state of the art. HgCdTe is the current choice material used in IR detectors. The material's bandgap can span the entire infrared regime allowing devices to operate in wavelengths from 1μm to 30μm. HgCdTe has some downfalls impacting device performance and cost. The substrates are expensive and II-VI material processing is not as advanced as its III-V counterpart[3–6]. The material itself also experiences inhomogeneity due to phase segregation into HgTe and CdTe regions[7]. Devices will also suffer from thermal expansion and Auger recombination events reducing efficiency [3–5]. HgCdTe is also a fragile material reducing device lifetime and has a low operating temperature requiring significant cooling[6]. The more robust capabilities in III-V semiconductor processing could improve many of these points once the required operating band gap is available, and the device performance holds up to current HgCdTe technologies.

1.3 Growth of Bismides

Currently III-V alloys containing Bi have proven difficult to grow often resulting in droplets on the surface[21,22]. The difficulty is expected due to the unstable nature of the endpoints of GaBi and InBi. To date, the most studied of the alloys is GaAsBi with reports showing up to 22% Bi incorporation with droplets on the surface and up to 11% with clean surfaces[23]. The weak Bi bond contributes to easily reaching the saturation point of Bi at the given set of growth conditions. There are two different saturations of Bi incorporation that can be considered, one is the maximum incorporation achievable at a given temperature and one is the maximum incorporation at a given V:III flux ratio which controls the availability of III sites for Bi to bond to. These two varieties of Bi saturation are seen in the graphs in Fig. 1-3 where the temperature series comes from Lu et al[24] and the V:III series comes from Lewis et al[23]. This provides a few possible actions to increase the Bi composition: increase the Bi flux if it is not saturated along that axis, reduce the V:III flux ratio if it isn't saturated along that axis, or reduce the growth temperature.

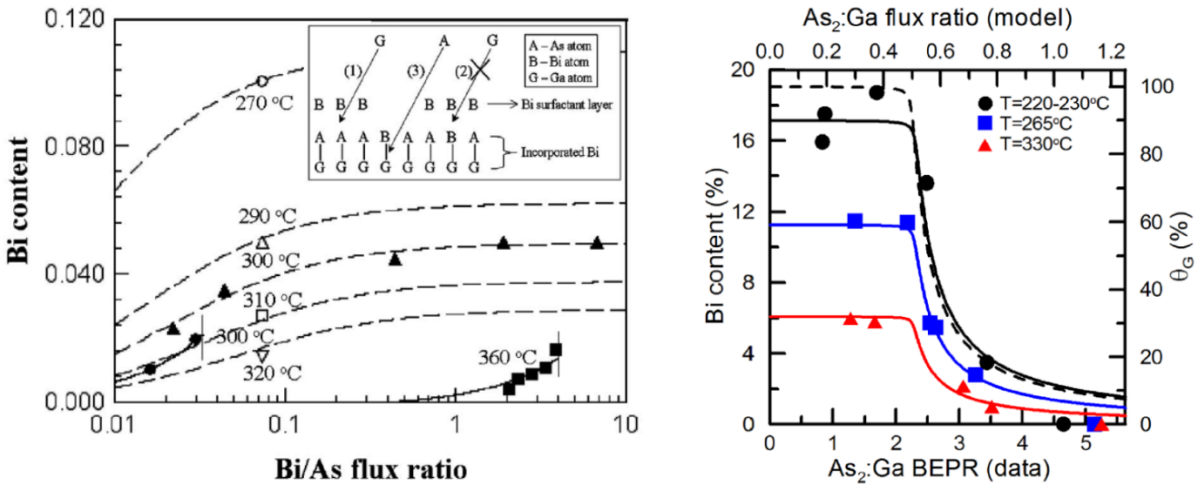

Figure 1-3: (left) Temperature series of GaAsBi with different Bi/As flux ratios, the inset is a model of the surfactant based growth for Bi incorporation from[24]; (right) Set of growths at 3 temperatures of 220-230°C, 265°C, and 330°C showing Bi content v. As:Ga beam equivalent pressure ratio(BEPR) with lines showing a model of the Ga coverage.[23]

More recently, GaSbBi has been studied with reports indicating Bi incorporation of up to 9.6%. It is also paired with photoluminescence data showing the expected smaller reduction in bandgap per percent Bi when compared to GaAsBi[25–29]. The Millunchick group's investigation of GaSbBi [21]shows varying amounts of Bi and Ga surface droplets as well as a propensity for background As to incorporate into the material through a proposed auto-strain compensation mechanism. Examples of both Ga and Bi droplets appearing on the surface can be found in Fig 1-4 with examples in GaAsBi and GaSbBi. Up until the work presented in this dissertation the impact of the droplets is unclear and it is possible if they are not deleterious in the growth of the material they could be handled by post processing the surface by etching the droplets away. In addition to these ternary alloys there has been some work on quaternary III-V alloys containing Bi where most work has occurred on InGaAsBi with up to a 7% Bi incorporation[30–32]. The quaternary alloys are the most promising alloys for future devices as they will be capable of having a range of operating wavelengths while remaining strain free on a select substrate. In

order to approach quaternary alloys it will be of great help to initially understand behavior of the ternary alloys.

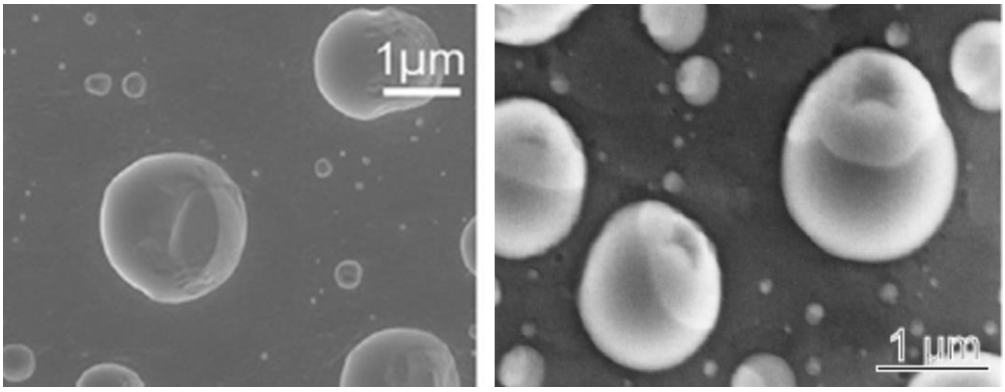

Figure 1-4: SEM images of biphasic Ga/Bi droplets on GaAsBi(left)[22] and GaSbBi(right)[21]

Along with the difficulty of finding optimal growth conditions for high incorporation and the appearance of droplets on the surface, GaAsBi has recently been shown to have an inhomogeneous distribution with an initial high concentration at the film substrate interface and reducing through the film's thickness [33,34]and has exhibited some various crystalline orderings[34–36]. Additionally, there have been investigations on the kinetics of the growth of GaAsBi with a proposed theoretical model. Ptak et al. [37]have shown that at low Bi flux the incorporation percentage increases linearly with the Bi flux and occurs at a slower rate for higher growth rates. There has been a proposed kinetic model initially reported by Lu et al. [24]and improved upon by Lewis et al.[23] capturing incorporation trends based on growth temperature and differences in the Ga:As flux ratio. The current issue with this model is that it does not allow or account for any droplets forming on the surface and does not capture the inhomogeneity observed in other publications.

1.4 Organization

The remainder of the dissertation is organized as follows:

Chapter 2 contains a discussion of the advances made to the Socorro density functional theory platform in order to perform ab initio calculations on the electronic structure of these alloys. The advances made include implementation of cell shape relaxation for eventual application in epitaxially strained cells, and implementation of Spin-orbit coupling for more accurate band structure calculations with cells containing large atoms such as Bi.

Chapter 3 is an investigation and formulation of the kinetics associated with Bismide growth. This is an extension of previous models guided by experiments in GaSbBi. The model changes how Bi is handled on the surface and accumulates into droplets. The Bi droplets are found to change the incorporation capability of Bi when present generating a need for an additional kinetic term. The model and it's impacts are corroborated with experiments in GaSbBi. The inhomogeneity found in this chapter is controlled simply by the presence of Bi droplets in the growth.

Chapter 4 focuses on the inhomogeneities found in Bismide growth. It contains two main sections. The first concerns inhomogeneities induced by the presence of Ga droplets. It shows that when Ga droplets are present on the surface there are up to three different incorporation rates for Bi resulting in stripe like inhomogeneities in the film. It shows that the inhomogeneity due to Ga droplets can potentially be controlled via growth interruptions. The second section is concerned with the inhomogeneities that appear in droplet free growth conditions. This section shows that reduction in growth temperature eventually results in roughening of the surface and appearance of a lateral composition modulation of Bi, Bi clusters, and nanopores. These inhomogeneities are linked to a decomposition of the surface by the varying diffusion rates of adatoms at the surface. These sections along with chapter 3 suggest that growth with droplets on the surface generates irreversible inhomogeneities in the Bi composition, and growths that are

droplet free need to maintain smooth surfaces or suffer from a different set of Bi inhomogeneities.

Chapter 5 touches on future growth directions and some results on GaAsBi/GaAs superlattices as a possible solution to the inhomogeneities discussed throughout the dissertation.

1.5 References

1. Schlenker, D., Miyamoto, T., Pan, Z., Koyama, F. & Iga, K. Miscibility gap calculation for Ga1−xInxNyAs1−y including strain effects. *J. Cryst. Growth* **196,** 67–70 (1999).
2. Sweeney, S. J., Member, S., Batool, Z., Hild, K. & Member, A. The Potential Role of Bismide Alloys in Future Photonic Devices. 4–7 (2011).
3. Norton, P. HgCdTe Infrared Detectors. *Opto-Electronics Rev.* **10,** 159–174 (2002).
4. Rogalski, a. HgCdTe infrared detector material: history, status and outlook. *Reports Prog. Phys.* **68,** 2267–2336 (2005).
5. Razeghi, M. & Nguyen, B.-M. Advances in mid-infrared detection and imaging: a key issues review. *Rep. Prog. Phys.* **77,** 82401 (2014).
6. Rogalski, A., Martyniuk, P. & Kopytko, M. Challenges of small-pixel infrared detectors: A review. *Reports Prog. Phys.* **79,** (2016).
7. Vasilevskiy, M. I. & Anda, E. V. Diffusion instability of homogeneous distribution of mercury in cadmium mercury telluride. *Semicond. Sci. Technol.* **10,** 157–162 (1999).
8. Pandya, G. R. & Vyas, S. M. Characteristic Growth Features and Etching of InBi Single Crystals. *Cryst. Res. Technol.* **28,** 163–167 (1993).
9. Tiedje, T., Young, E. C. & Mascarenhas, A. Growth and properties of the dilute bismide semiconductor GaAs1−xBix a complementary alloy to the dilute nitrides. *International Journal of Nanotechnology* **5,** 963 (2008).
10. Bertulis, K. *et al.* GaBiAs: A material for optoelectronic terahertz devices. *Appl. Phys. Lett.* **88,** 201112 (2006).
11. Lu, X., Beaton, D. a., Lewis, R. B., Tiedje, T. & Zhang, Y. Composition dependence of photoluminescence of GaAs1−xBix alloys. *Appl. Phys. Lett.* **95,** 41903 (2009).
12. Pačebutas, V., Bertulis, K., Aleksejenko, G. & Krotkus, a. Molecular-beam-epitaxy grown GaBiAs for terahertz optoelectronic applications. *J. Mater. Sci. Mater. Electron.* **20,** 363–366 (2009).
13. Pettinari, G. *et al.* Effects of Bi incorporation on the electronic properties of GaAs: Carrier masses, hole mobility, and Bi-induced acceptor states. *Phys. Status Solidi* **250,** 779–786 (2013).
14. Wu, J., Shan, W. & Walukiewicz, W. Band anticrossing in highly mismatched III V

semiconductor alloys. *Semicond. Sci. Technol.* **17,** 860–869 (2002).

15. Alberi, K. *et al.* Valence-band anticrossing in mismatched III-V semiconductor alloys. *Phys. Rev. B* **75,** 45203 (2007).

16. Cooke, D. G., Hegmann, F. a., Young, E. C. & Tiedje, T. Electron mobility in dilute GaAs bismide and nitride alloys measured by time-resolved terahertz spectroscopy. *Appl. Phys. Lett.* **89,** 140–142 (2006).

17. Fluegel, B. *et al.* Giant Spin-Orbit Bowing in GaAs1-xBix. *Phys. Rev. Lett.* **97,** 67205 (2006).

18. Mazur, Y. I. *et al.* Effects of spatial confinement and layer disorder in photoluminescence of GaAs 1− x Bi x /GaAs heterostructures. *J. Phys. D. Appl. Phys.* **46,** 65306 (2013).

19. Yoshida, J., Kita, T., Wada, O. & Oe, K. Temperature Dependence of GaAs 1- x Bi x Band Gap Studied by Photoreflectance Spectroscopy. *Jpn. J. Appl. Phys.* **42,** 371–374 (2003).

20. Pursley, B., Luengo-Kovac, M., Vardar, G., Goldman, R. S. & Sih, V. Spin lifetime measurements in GaAsBi thin films. *Appl. Phys. Lett.* **102,** 22420 (2013).

21. Duzik, A. & Millunchick, J. M. Surface morphology and Bi incorporation in GaSbBi(As)/GaSb films. *J. Cryst. Growth* **390,** 5–11 (2014).

22. Vardar, G. *et al.* Mechanisms of droplet formation and Bi incorporation during molecular beam epitaxy of GaAsBi. *Appl. Phys. Lett.* **102,** 42106 (2013).

23. Lewis, R. B., Masnadi-Shirazi, M. & Tiedje, T. Growth of high Bi concentration GaAs1−xBix by molecular beam epitaxy. *Appl. Phys. Lett.* **101,** 82112 (2012).

24. Lu, X., Beaton, D. a., Lewis, R. B., Tiedje, T. & Whitwick, M. B. Effect of molecular beam epitaxy growth conditions on the Bi content of GaAs[sub 1−x]Bi[sub x]. *Appl. Phys. Lett.* **92,** 192110 (2008).

25. Song, Y., Wang, S., Saha Roy, I., Shi, P. & Hallen, A. Growth of GaSb1−xBix by molecular beam epitaxy. *J. Vac. Sci. Technol. B Microelectron. Nanom. Struct.* **30,** 02B114 (2012).

26. Rajpalke, M. K. *et al.* Growth and properties of GaSbBi alloys. *Appl. Phys. Lett.* **103,** 142106 (2013).

27. Rajpalke, M. K. *et al.* High Bi content GaSbBi alloys. *J. Appl. Phys.* **116,** 43511 (2014).

28. Wang, S., Song, Y. & Roy, I. S. Bismuth incorporation and lattice contraction in GaSbBi and InSbBi. *2011 13th Int. Conf. Transparent Opt. Networks* **3,** 1–3 (2011).

29. Das, S. K., Das, T. D. & Dhar, S. Effect of post-growth anneal on the photoluminescence properties of GaSbBi. *Semicond. Sci. Technol.* **29,** 15003 (2014).

30. Feng, G., Yoshimoto, M., Oe, K., Chayahara, A. & Horino, Y. New III-V semiconductor InGaAsBi alloy grown by molecular beam epitaxy. *Japanese J. Appl. Physics, Part 2 Lett.* **44,** 0–3 (2005).

31. Zhong, Y., Dongmo, P. B., Petropoulos, J. P. & Zide, J. M. O. Effects of molecular beam epitaxy growth conditions on composition and optical properties of InxGa1−xBiyAs1−y. *Appl. Phys. Lett.* **100,** 112110 (2012).

32. Devenson, J., Pačebutas, V., Butkute, R., Baranov, A. & Krotkus, A. Structure and optical properties of InGaAsBi with up to 7% bismuth. *Appl. Phys. Express* **5,** 8–11 (2012).

33. Reyes, D. F. *et al.* Bismuth incorporation and the role of ordering in GaAsBi/GaAs structures. *Nanoscale Res. Lett.* **9,** 23 (2014).

34. Mohmad, a R. *et al.* Bismuth concentration inhomogeneity in GaAsBi bulk and quantum well structures. *Semicond. Sci. Technol.* **30,** 94018 (2015).

35. Wu, M., Luna, E., Puustinen, J., Guina, M. & Trampert, A. Observation of atomic ordering of triple-period-A and -B type in GaAsBi. *Appl. Phys. Lett.* **105,** (2014).

36. Norman, A. G., France, R. & Ptak, A. J. Atomic ordering and phase separation in MBE GaAs1−xBix. *J. Vac. Sci. Technol. B, Nanotechnol. Microelectron. Mater. Process. Meas. Phenom.* **29,** 03C121 (2011).

37. Ptak, A. J. *et al.* Kinetically limited growth of GaAsBi by molecular-beam epitaxy. *J. Cryst. Growth* **338,** 107–110 (2012).

Chapter 2: Adapting Socorro: A Density Functional Theory Platform for Calculations on Bismides

2.1 Introduction

The bismides are currently unknown territory for III-V material development. The speed at which this material is developed will be determined by how quickly we can understand and control the phenomena associated with their growth. Computational methods provide a useful avenue to speed discovery in materials development.

Density functional theory (DFT) is a computational quantum mechanical model generally used for calculation of ground state electron density of many-body systems. It has proven itself as a useful tool for characterizing and understanding a wide variety of material systems. DFT is often used for evaluating ground state configurations, like the bandgap of various semiconductor configurations or the preferred cell shape and atomic positions. DFT calculations, however, can be computationally expensive depending on the size of the computational cell and the functional that is used. Functionals are approximations used for modelling the exchange and correlation interactions of electrons and vary in accuracy and computational expense. Conventional DFT functionals give vanishing band gaps for narrow band gap semiconductors such as InAs, GaSb, InSb, and III-V-Bi. The metallic character of these materials when treated with conventional DFT leads to errors in the occupation of surface states and the screening of Coulomb interactions between separated charges. In recent years, increasingly accurate DFT calculations have been

performed using hybrid functionals, which can yield accurate results even for narrow band gap materials.

Computational investigation of the III-V-Bi alloys is critical for their development because of the unstable nature of the Bi endpoints. GaBi is not stable and cannot be isolated experimentally. This means simple estimations like the alloy lattice constant through Vegard's law is impossible without a lattice constant for GaBi determined through computation. The GaBi and InBi endpoint structures have been calculated to estimate their zincblende lattice parameter and is used to estimate compositions of the various III-V-Bi alloys[1]. Structural and electronic characterization of these alloys through computation will expediate experimental development.

There are a few examples of recent computational investigation of III-V-Bi alloys. One group has studied GaAsBi with the local density approximation (LDA)[2] and Perdew-Burke-Ernzerhof (PBE) generalized gradient approximation (GGA)[3] using the Vienna ab initio simulation package (VASP). They found that Bi does not have a preference to cluster as well as investigating some of the thermodynamics of mixing for the alloy [4,5]. They also found that Ga vacancy concentration might be increased by the incorporation of Bi. Another group used LDA with VASP to find that the equilibrium solubility of Bi in GaAs increases when GaAs is put under tensile strain but is insufficient to explain experimentally obtained compositions[6]. The downfall of any LDA or GGA method for these materials is that investigating the band structure for the alloys is impossible due to the band gap collapsing. Collapse of the bandgap restricts the calculations from determining the effect the favored arrangement of Bi atoms and vacancies has on the electronic structure. While the structural properties have been more expansively

investigated the bandgap collapse limits computational investigation into the electronic properties.

Another group has utilized the Heyd-Scuseria-Ernzerhof (HSE) hybrid functional in VASP to avoid the band gap collapse and using it to investigate the crystal structure, band gap energy, and elastic coefficients[7]. The alloying is investigated using coarse alloying steps of 1/16, which would miss any possible nuance in the electronic structure for smaller compositions. This is likely as large of cells they could feasibly use before the calculations become too computationally expensive. The ability to perform electronic structure calculations on larger cells with accurate band gaps represents a step forward in the field.

Socorro is a computational platform developed at Sandia National Laboratories that has better scaling for the HSE functionals potentially allowing for finer steps in composition. Scaling in this context refers to how well a given code performs a calculation with an increase in number of cores used. Socorro is however missing some critical features for undertaking these calculations, cell shape relaxation and spin-orbit coupling. This chapter discusses implementation of these two critical features and the initial steps towards a computational investigation of III-V-Bi alloys.

2.1.1 Socorro

Socorro is a highly scalable DFT electronic-structure code. The code can be used to perform spin-polarized and non-spin-polarized DFT calculations in a plane-wave basis using norm-conserving pseudopotentials (NCPs)[8] or projector-augmented-wave (PAW)[9] potentials to model the ions and core electrons, and density-dependent functionals from the LibXC library[10] to describe exchange and correlation effects among valence electrons. In addition, NCP-based calculations can be performed using LibXC hybrid functionals, which combine density- and

orbital-dependent exact-exchange with density-dependent correlation. In this case, novel algorithms are used to construct and apply the exact-exchange operator, allowing the use of significantly more processing cores than are currently allowed with commercial and academic electronic structure codes. This translates to a high scalability of Socorro with hybrid functionals and is demonstrated with near optimal time vs. number of cores on a 256 atom cell of gold using HSE in Figure 2-1.

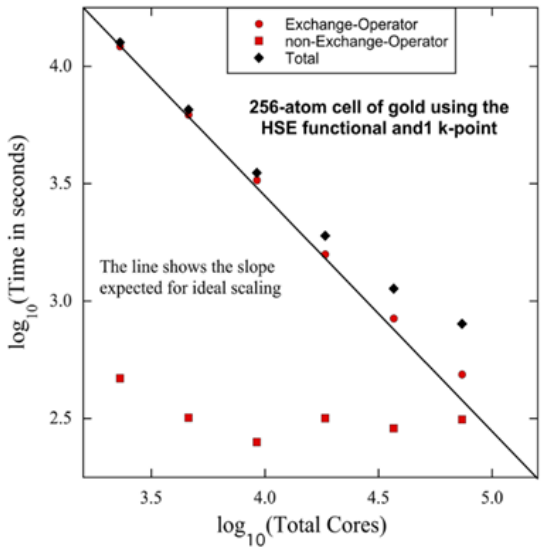

Figure 2-1: Scaling of a calculation of a 256 atom cell of gold using HSE with 1 k-point sampling, and 2034 Kohn-Sham orbitals showing a near linear scalingup to 73728 cores

The efficient scaling in Socorro with hybrid functionals means bismides can be calculated in a more complete fashion than demonstrated in previous works while minimizing problems like the band gap collapse because of the ability to scale to larger computational cells. Socorro was missing a few critical features to perform meaningful calculations on Bi containing III-V materials. The first is cell shape relaxation, which is an important parameter for understanding how strain effects the behavior of these materials. Also, Bi incorporation will greatly increase the spin-orbit coupling in these materials. This implies that for accurate calculations, spin-orbit

coupling will have to be included to predict the impact Bi incorporation has on the band structure. The remainder of this chapter outlines adding these two pieces of functionality to the Socorro code.

2.2 Cell shape Relaxation

Socorro was previously missing an internal cell shape optimization routine requiring any lattice optimization to be done in individual steps. This means that cell shape optimization requires running individual energy calculations on a variety of cell sizes and determining the minimum energy, as opposed to changing the cell shape while performing the energy minimization the calculation does. This effect would make investigating large numbers of configurations difficult due to the time and number of individual steps.

Implementation of cell shape relaxation was relatively straightforward since Socorro already calculated the stress tensor, it was merely a problem of using the stress for cell shape optimization. Following the definitions set forth in Bucko et al.[11] and basic elastic theory, steps for lattice optimization are calculated from the given stress tensor, σ, assuming the relaxation step occurs in the same direction as the stress. These steps are iterated through until the stress tensor is minimized.

Epitaxial strain is another condition that would be interesting simulate since the bismides have a significant lattice mismatch to most substrates they could be grown on given the calculated lattice constant of GaBi. This form of strain is simply a cell that is confined along two axes while one axis relaxes fully. The implementation is a straightforward extension of the previously mentioned cell shape relaxation procedure. Instead of using the entire stress tensor, σ,

only a single column of σ is minimized. A visualization of the three possible cell shape relaxation conditions can be found in Fig. 2-2.

2.2.1 Investigation of Epitaxial Strain impacts on ordering in GaAsBi

Cell shape relaxation in Socorro allowed for probing the impacts of epitaxial strain in the ground state configurations in GaAsBi. GaAsBi has been shown to exhibit $CuPt_b$ type ordering in some thin film growths[12,13]. The ordering is either a global energy minimum or a trapped state in a local minimum. DFT calculations on the ordered phases with and without epitaxial strain should provide some insight on which energy state the ordering is associated with.

All symmetry unique supercells of GaAsBi with Bi substituting on group V sites were generated up to a supercell size of 5 or 10 atoms. DFT formation energies of each possible configuration was run utilizing the PBE GGA functional with 3 different cell relaxation conditions seen in Fig. 2-2. The conditions for the lattice relaxation were fully constrained to GaAs lattice constant, fully relaxed, and relaxed in a single axis to represent epitaxial strain of growth on a (001) GaAs substrate illustrated in the right of Fig. 2-2. The formation energies were calculated relative to the two reference endpoints of GaAs and GaBi and plotted in Fig. 2-2. Each point in the plot represents one of the symmetry unique configurations possible for a given composition of GaAsBi.

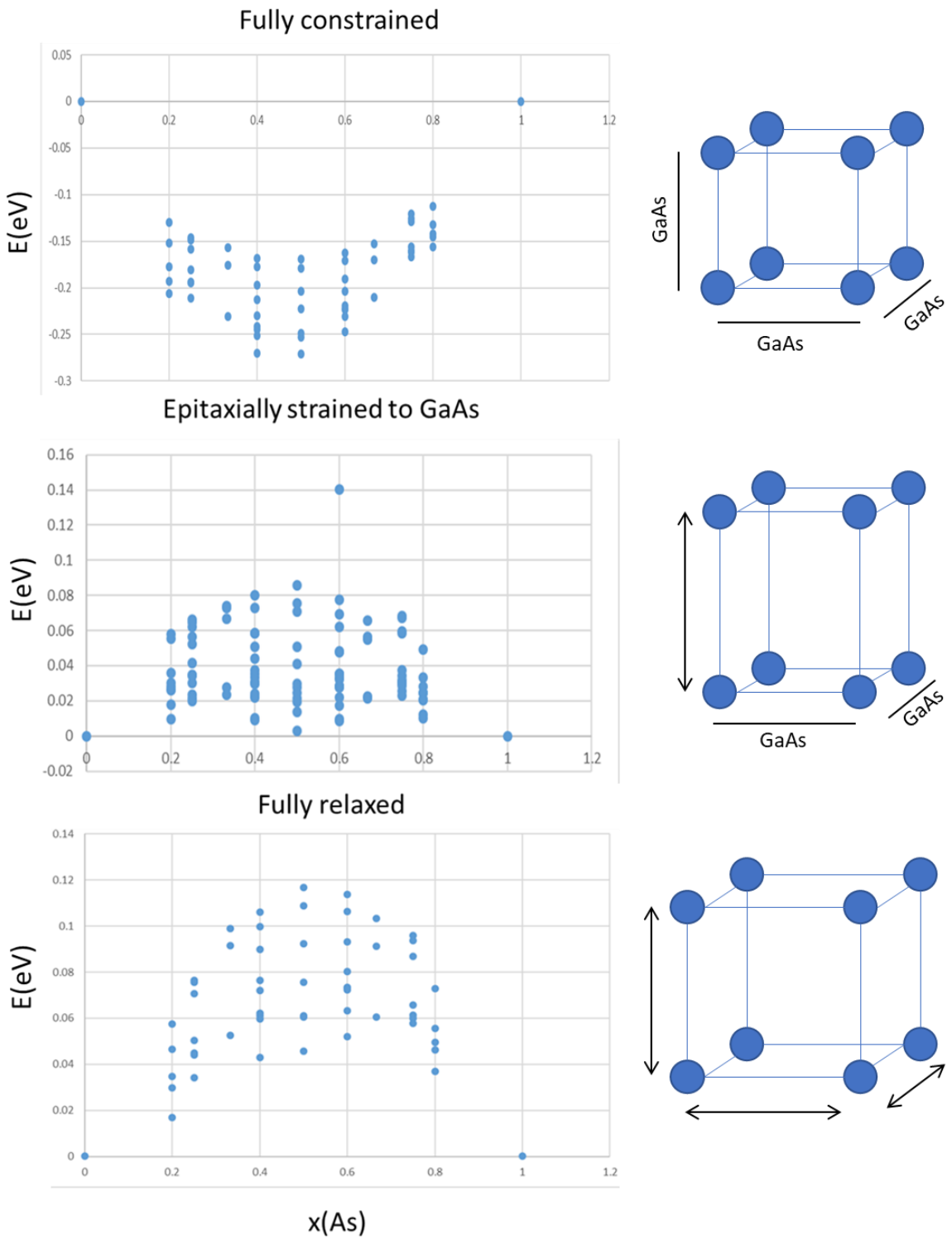

Figure 2-2: DFT Formation energies for GaAsBi under various cell shape relaxation conditions referenced to the two endpoint compounds(left). Depiction of relaxation restrictions on the cubic lattice where arrowheads indicate an axis that is free to relax.(right)

The fully constrained case is a reference for the most stabilized the ordered phases could be with ordered phases of 60% and 50% being the lowest in energy at ~.27eV. A lattice that is fully constrained to GaAs lattice constants is not physical in regards to film growth. The calculation with full constraints merely illustrates a situation that is most conducive for stable ordered phases. For the epitaxial constraint, the energies of the ordered phases are closer to the reference states but are still unstable relative to the reference energy. The closest to stabilized is a 50% Bi phase at ~3meV from the reference state. The fully relaxed condition shows that none of the configurations are favored over the two endpoints. These results fall in agreement with Punkinnen et al. where they found LDA and PBE calculation on special quasi-random structures had the totally disordered alloys as the most stable[5]. The results of these calculations provide good proof of concept that the cell shape relaxation can enable exploration of different strain states once band structure calculations can be done in Socorro. For the band gap calculations to be done, spin-orbit coupling must first be implemented into Socorro. The following section outlines the contributions towards spin-orbit coupling in Socorro.

2.3 Spin-orbit coupling

Spin-orbit coupling is the relativistic effect associated with the spin of the electron coupling to the motion associated with its orbit. The magnitude of the spin orbit coupling potential, V_{SO}, is proportional to the angular momentum operator dotted into the spin angular momentum operator.

$$V_{SO} \; \alpha \; L \cdot S$$

Spin-orbit coupling becomes larger while going down the periodic table. Bi incorporation even in small amounts would be expected to drastically increase the spin-orbit

coupling term in a given III-V alloy. Any DFT-based investigation into the electronic structure of these materials would need to include spin-orbit coupling for a good approximation of their behavior.

The goal is to add an implementation of spin-orbit coupling into Socorro to take advantage of it's high scalability with hybrid functionals to calculate the electronic structure across a range of experimentally accessible III-V-Bi configurations. The implementation requires a relativistic pseudopotential be available which was previously missing in the Socorro code.

2.3.1 Pseudopotential Addition

Socorro needed to handle a norm-conserving pseudopotential that is relativistic and is optimized for the PBE GGA functional. We incorporated the pseudopotentials developed by Hartwigsen, Goedecker, and Hutter[14,15] which were originally constructed for use with the LDA functional but was later optimized for PBE by Krack[16]. The pseudopotentials were appealing to implement for a few reasons. One reason is that they are separable into individual contributions for the local, nonlocal associated with scalar relativistic effects, and the nonlocal spin orbit interaction. Another appealing reason is the pseudopotentials are analytic meaning that they only need a set of input parameters as opposed to a grid of values that would have to be splined to determine values for a given wavevector.

The total pseudopotential is given by,

$$V(r,r') = V_{loc}(r)\delta(r-r') + \sum_{l} V_l(r,r') + \Delta V_l^{SO}(r,r')L \cdot S$$

where V_{loc} is a local piece with a form that can be found in the originating paper[14]. V_l and ΔV_l^{SO} are very similar. The form for V_l is:

$$V_l(r,r') = \sum_{i=1}^{3}\sum_{j=1}^{3}\sum_{m=-l}^{+l} Y_{l,m}(\hat{r})p_i^l(r)h_{i,j}^l p_j^l(r')Y_{l,m}^*(\hat{r}')$$

where $Y_{l,m}$ are the spherical harmonics, and l the angular momentum quantum number. $p_i^l(r)$ are projectors that are Gaussian in form. ΔV_l^{SO} is the same as $V_l(r,r')$ except $h_{i,j}^l$ is replaced with a different set of constants $k_{i,j}^l$. These constants are input parameters that are read in when initializing the pseudopotential in Socorro.

The projectors were imported in their reciprocal space form since this is the primary space that Socorro operates in. An example of the reciprocal space projectors is as follows:

$$p_1^{l=0} = \frac{4\sqrt{2r_0^3}\pi^{5/4}}{\sqrt{\Omega}\exp[\frac{1}{2}(gr_0)^2]}$$

$$p_1^{l=1} = \frac{8\sqrt{\frac{r_1^5}{3}}\pi^{5/4}g}{\sqrt{\Omega}\exp[\frac{1}{2}(gr_1)^2]}$$

$$p_1^{l=2} = \frac{8\sqrt{\frac{2r_2^5}{15}}\pi^{5/4}g^2}{\sqrt{\Omega}\exp[\frac{1}{2}(gr_2)^2]}$$

where Ω is the cell volume and the r's are an input parameter associated with the pseudopotential input file. An important note is that these projectors have a factor of g^l in them which is already incorporated in the Socorro spherical harmonics. Because of this the projectors within Socorro differ from the ones found in the source paper by g^l.

Another feature that is new in these pseudopotentials is multiple channels for a given value of l. Handling this for a norm conserving pseudopotentials was previously not available in

Socorro and the feature was added. The scalar relativistic portions of the pseudopotential was tested against other norm conserving pseudopotentials to check that the application of the multiple channels and projector functions was done correctly.

In order to apply the non-scalar parts of the pseudopotentials Socorro must be made to handle two different spin densities to have them interact and mix from $L \cdot S$. This addition requires changes in the more complicated backend of Socorro and is being incorporated by Normand Modine and Alan Wright at Sandia National Laboratory.

The final addition made to the Socorro code was the application of $L \cdot S$ at the pseudopotential handling level assuming that the two relevant spin pieces are passed down. The application is a straightforward application of the operators for $L \cdot S$.

$$L \cdot S = \frac{1}{2}\begin{pmatrix} L_z & L_- \\ L_+ & -L_z \end{pmatrix}$$

where L_- and L_+ are the raising and lowering operators with the following eigenvalues:

$$L_\pm \psi_{lm} = \sqrt{l(l+1) - m(m \pm 1)}\psi_{lm\pm1}$$

and:

$$L_z \psi_{lm} = m\psi_{lm}$$

2.4 Future Work and Initial Calibrations

The first set of calculations that is sensible to attempt once Socorro is fully operating with spin-orbit coupling would be to generate large GaAsBi cells either 128 atoms or 256 atoms and calculate the band structure. The cells could be generated with Monte Carlo trajectories with the cluster assisted statistical mechanics package utilized in the groups previous surface reconstruction efforts[17]. This approach will allow calculation of the band structures of cells that

are more likely to appear in reality since temperature can play a role in accessing favorable arrangements of Bi in GaAs. The calculations would be done using HSE functionals with mixing to match the experimental bandgap of GaAs that has its cell shape relaxed via PBE functional calculations. This would be done in this manner because relaxation with the HSE functionals would be very computationally expensive and Socorro is currently missing implementation for cell relaxation with the hybrids. It is reasonable to do this because the lattice constant difference between relaxing with PBE vs. HSE is relatively small ~1% and the difference in the optimal mixing in HSE for the two possible cell relaxation cases is small 0.3 for PBE relaxed versus 0.26 for HSE relaxed.

These calculations can be a vaulting point for understanding the band structure impacts of incorporating Bi in a multitude of III-V systems in the small percentages that have been accessed through experiments. With Socorro fully equipped to handle these calculations it will be the perfect addition to experimental thrusts in developing and understanding the III-V-Bi alloys.

2.5 References

1. Janotti, a., Wei, S.-H. & Zhang, S. Theoretical study of the effects of isovalent coalloying of Bi and N in GaAs. *Phys. Rev. B* **65,** 115203 (2002).
2. Perdew, J. P. & Zunger, A. Self-interaction correction to density-functional approximations for many-electron systems. *Phys. Rev. B* **23,** 5048–5079 (1981).
3. Perdew, J. P., Burke, K. & Ernzerhof, M. Generalized gradient approximation made simple. *Phys. Rev. Lett.* **77,** 3865–3868 (1996).
4. Punkkinen, M. P. J. *et al.* Does Bi form clusters in GaAsBi alloys? *Semicond. Sci. Technol.* **29,** 115007 (2014).
5. Punkkinen, M. P. J. *et al.* Thermodynamics of the pseudobinary GaAs<inf>1-x</inf>Bi<inf>x</inf> (0 ??? x ??? 1) alloys studied by different exchange-correlation functionals, special quasi-random structures and Monte Carlo simulations. *Comput. Condens. Matter* **5,** 7–13 (2015).
6. Jacobsen, H., Puchala, B., Kuech, T. F. & Morgan, D. Ab initio study of the strain dependent thermodynamics of Bi doping in GaAs. *Phys. Rev. B* **86,** 85207 (2012).
7. Cao, H., Yu, Z., Lu, P., Chen, J. & Wang, S. Hybrid functional investigations of the

crystal structure, band gap energy, and elastic coefficients of GaAs1-xBix solid solutions. *Comput. Mater. Sci.* **105,** 6–10 (2015).

8. Hamann, D., Schlüter, M. & Chiang, C. Norm-Conserving Pseudopotentials. *Phys. Rev. Lett.* **43,** 1494–1497 (1979).

9. Blochl, P. E. Projector augmented-wave method. *Phys. Rev. B* **50,** 17953 (1994).

10. Marques, M. A. L., Oliveira, M. J. T. & Burnus, T. Libxc: A library of exchange and correlation functionals for density functional theory. *Comput. Phys. Commun.* **183,** 2227–2281 (2012).

11. Bucko, T., Hafner, J. & Angyán, J. G. Geometry optimization of periodic systems using internal coordinates. *J. Chem. Phys.* **122,** 124508 (2005).

12. Norman, A. G., France, R. & Ptak, A. J. Atomic ordering and phase separation in MBE GaAs1−xBix. *J. Vac. Sci. Technol. B, Nanotechnol. Microelectron. Mater. Process. Meas. Phenom.* **29,** 03C121 (2011).

13. Reyes, D. F. *et al.* Bismuth incorporation and the role of ordering in GaAsBi/GaAs structures. *Nanoscale Res. Lett.* **9,** 23 (2014).

14. Hartwigsen, C., Goedecker, S. & Hutter, J. Relativistic separable dual-space Gaussian pseudopotentials from H to Rn. **58,** (1998).

15. Goedecker, S., Teter, M. & Hutter, J. Separable dual-space Gaussian pseudopotentials. *Phys. Rev. B* **54,** 1703–1710 (1996).

16. Krack, M. Pseudopotentials for H to Kr optimized for gradient-corrected exchange-correlation functionals. *Theor. Chem. Acc.* **114,** 145–152 (2005).

17. Thomas, J. C., Millunchick, J. M., Modine, N. A. & Van Der Ven, A. Surface atomic order of compound III-V semiconductor alloys at finite temperature. *Phys. Rev. B - Condens. Matter Mater. Phys.* **80,** 1–12 (2009).

Chapter 3: Kinetics of III-V-Bi Growth

3.1 Introduction

Controlled growth of difficult materials like the III-V-Bi alloys requires high control over all interacting phenomena present during growth. Well-characterized kinetic models capture these interacting phenomena and provide insight on effective growth parameter ranges for desired compositional effects.

This chapter investigates the kinetics and resulting impacts of Bi surface buildup during the growth of Bi-containing III-V compound semiconductor alloys. It develops a kinetic model that predicts droplet formation trends in these alloys, with experimental validation in the GaSbBi system. The model also predicts that droplet formation under certain growth conditions leads to compositional nonuniformity, in agreement with experimental observations in GaAsBi[1,2] and GaSbBi.

3.2 Experimental Methods

For the remainder of this dissertation, experimental methods will be described at the beginning of each chapter as they are used. Molecular beam epitaxy (MBE), scanning electron microscopy (SEM), energy dispersive spectroscopy (EDS), and x-ray diffraction (XRD) will be covered in this chapter. Atom probe tomography (APT) and transmission electron microscopy (TEM) descriptions can be found in chapter 4.

3.2.1 Molecular Beam Epitaxy (MBE)

All samples were grown via MBE in an EPI 930 chamber. Ga and Bi were provided by Knudsen effusion cells, with Ga having 2 heating zones and Bi having a single heating zone. As and Sb sources were provided by valved cracker sources. Sb was cracked at 900°C, As was either cracked at 600°C for As_4 or 1000°C for As_2. Beam equivalent pressures (BEP) were measured with a nude Bayard-Alpert ionization gauge that is placed directly in the path of the elemental sources to the sample position. Reflection high energy electron diffraction (RHEED) was used for in situ monitoring of surface oxide desorption, surface reconstruction and general surface quality during growth. RHEED oscillations were used to determine effective Ga, As, and Sb deposition rates. Growth temperature was monitored by an optical pyrometer with an operational detection range of 250°C-1400°C. Exact growth conditions of samples will be tabulated or enumerated as they are discussed in each chapter.

3.2.2 Characterization

Surfaces of samples were observed utilizing Scanning Electron Microscopy (SEM). This technique allows us to identify the broad surface quality of the samples. Droplet existence and coverage was ascertained from SEM. Characteristic x-rays from Bi and Ga were used to identify the composition of the droplets on the surface. This technique is Energy Dispersive Spectroscopy (EDS) and was done in tandem while taking the SEM images analyzed in the remainder of this dissertation.

All x-ray diffraction (XRD) presented was obtained on a Bede D1 high resolution x-ray diffractometer using Cu Kα radiation. When counts permitted, XRD traces were taken with triple axis measurement. Most analysis presented within this dissertation was obtained from diffraction from the (004) plane for either GaSb or GaAs. The diffraction traces are a critical

tool for identifying the Bi composition percentage and a guide for film homogeneity. Bi composition was estimated by assuming the crystal behaved within Vegard's law with a GaBi lattice parameter of 6.33Å that was obtained computationally[3].

Rutherford Backscattering Spectroscopy (RBS) is a technique that utilizes the ideas set forth in the classical Rutherford experiment. A sample is bombarded with high energy alpha particles and the resultant backscattering profile is measured and fitted to a sample profile. The energy loss of the scattering event is dependent on the individual nuclei mass allowing for identification of elemental composition of a given sample film.

The technique proved to be problematic for characterizing bismide films with multiple compositions and/or droplets on the surface. Figures 3-1 and 3-2 are 2 different fits of the same spectrum of a GaSbBi sample that was grown. Fits are done using the SimNRA software and only has a fitting algorithm for a single film so any films with multiple compositions must be fit by hand. This lead to two possible fits with significantly different implications of the Bi distribution in the film. The fit that was decided to be most sensible is Fig. 3-2 due to the better fit in the Bi edge of the spectrum. Due to the problematic fitting RBS was not used on any other samples since it was not clear that films with changing composition could be identified conclusively. If bismide material growth improves such that the surface is droplet free and the composition is homogeneous throughout the samples thickness, then RBS will be a useful characterization technique for corroborating the composition profile.

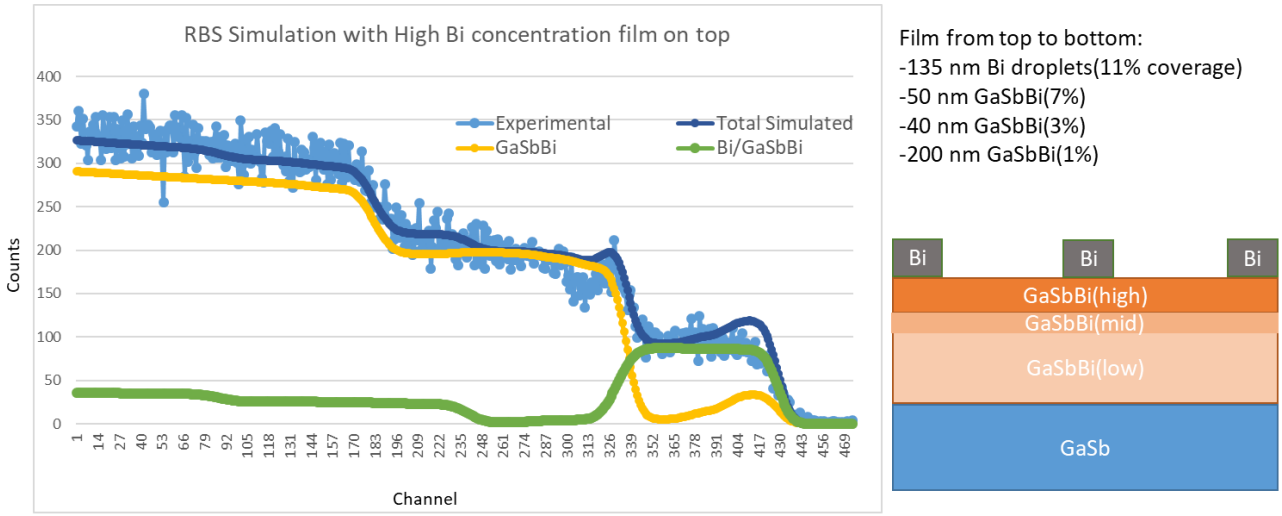

Figure 3-1: RBS spectrum profile and simulated fit for GaSbBi film with composition distributed with Bi droplets on the surface and the high Bi concentration film closer to the surface.

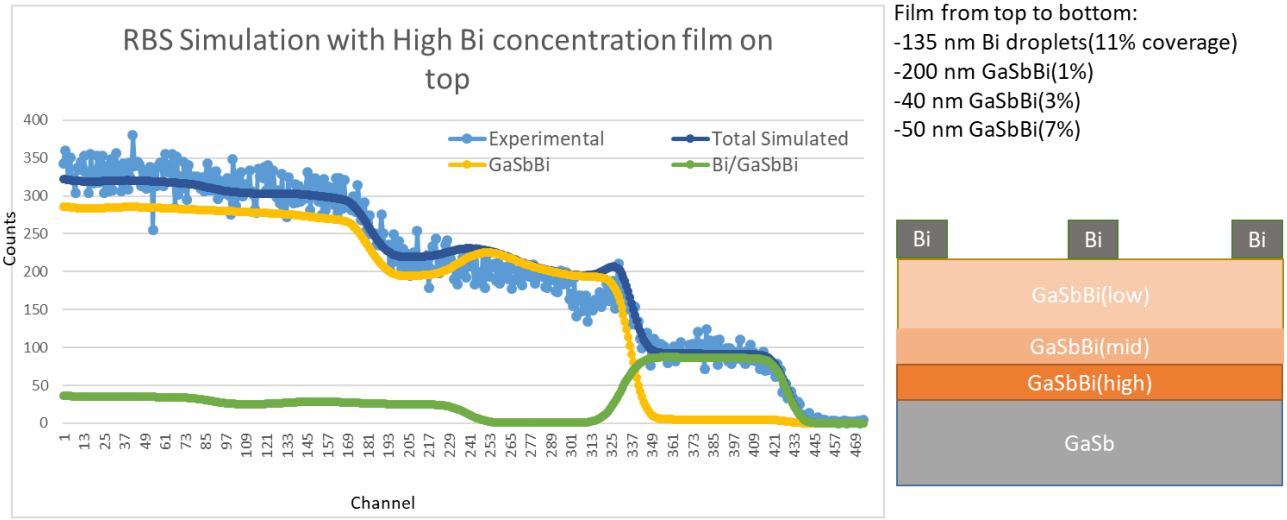

Figure 3-2: RBS spectrum profile and simulated fit for GaSbBi film with composition distributed with Bi droplets on the surface and the high Bi concentration film closer to the substrate.

3.3 Targeting Growth Parameters Using Surface Reconstructions

The initial experimental goals are to maximize the incorporation of Bi while maintaining a clean surface. It is known that the traditional binary systems of GaSb and GaAs grow optimally under Group V-rich conditions. This idea provides an initial target for the clean surfaces requirement as it prevents the occurrence of Ga droplets on the surface while being in a growth regime that is known for better material quality. To achieve the maximal Bi incorporation condition in these V-rich conditions, surface reconstructions can be used as a guiding measure.

Previous work in the group by Adam Duzik was focused on calculating the surface phase diagrams of GaSbBi[4] and GaAsBi[5,6]. Figure 3-3 is the calculated 0 K surface phase diagram for Bi/GaSb accompanied with some selected surface reconstructions. Maximizing the Bi in the surface reconstruction should lead to the highest possible Bi incorporation in the bulk film. This intuitively occurs at high Bi flux according to Fig. 3-3. Experimentally a 1x5 reconstruction was accessible at our growth temperatures of 305°C which is likely to be the 2x10 reconstruction that is discussed in Duzik et al.[4]. Bi in the surface reconstruction is maximized by crossing the boundary into the 1x5 reconstruction with the addition of the Bi flux. This methodology is effectively moving vertically across a boundary in the surface phase diagram in Fig 3-3.

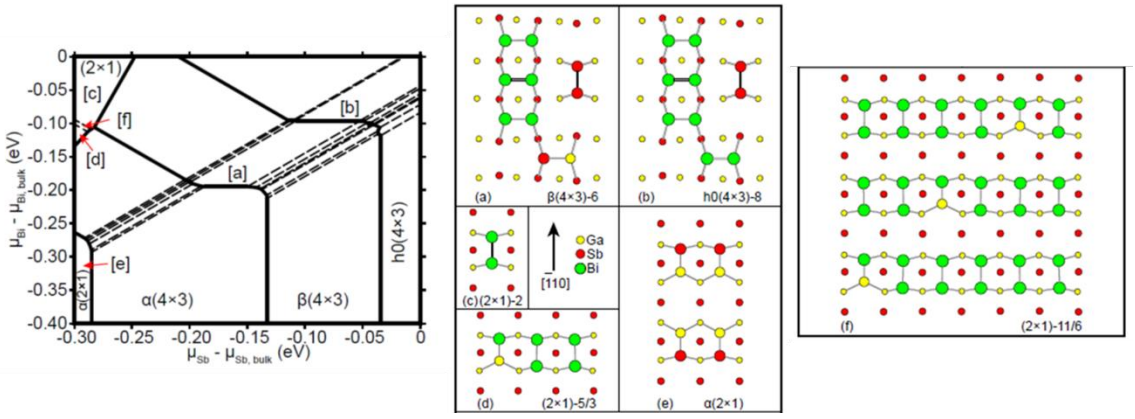

Figure 3-3: Calculated 0 K surface phase diagram for Bi/GaSb (left), Selected reconstructions associated with the surface phase diagram (middle and right).[4]

Growths of GaSbBi alloys in Sb-rich conditions did not lead to appreciable Bi incorporation. This can be explained by the surface reconstructions themselves. The reconstructions in the group V rich region have a characteristic double anion layer. Bi is always found to be on the topmost layer in the double anion layer. It would be difficult for Bi to incorporate with its weak bonding energy relative to the As or Sb in the lower layer leading to Bi not incorporating and just riding on the surface like a surfactant. The lack of incorporation in the group V-rich regime agrees with the model set forth by Lewis et al[7] which shows a drop off in Bi incorporation at high group V:Ga ratios. The advantageous aspect of these growth conditions is that the dynamics of surface Bi and its incorporation can be investigated without surface Ga buildup.

3.4 Kinetic Growth Model for III-V-Bi

Achieving high incorporation of Bi into GaAs or GaSb has been difficult. A common problem in growth of these films is droplets on the surface[8–10]. The highest reported Bi incorporation in GaAs is 22% with droplets, and up to 11% without droplets[7]. In GaSb, the highest reported Bi incorporation is 9% with clean surfaces[11]. There are also reports indicating varying incorporation over the thickness of GaAsBi films. For instance, Reyes et al. reports a 6% Bi

concentration near the film-substrate interface that decreases to ~2% over the remaining thickness of the film[1].

The kinetics of the Bi incorporation process has been studied by Lu et al.[12], who show how incorporation varies across different temperature growths resulting in a higher possible incorporation with lower growth temperatures. They also show lower Bi:As ratios are required to saturate the incorporation at lower growth temperatures. Ptak et al.[9] examined the effect of Ga rate on incorporation, demonstrating higher Bi flux requirements for similar incorporation percentages with higher Ga rates. Additionally, they show a trend of higher Bi flux requirements for droplets to form at higher fluxes[9]. Lewis et al.[7] expand on the model of Lu et al.[12] with experiments showing the dependence of Bi incorporation on Ga site availability. This model suggests that maximal Bi incorporation occurs at near or below stoichiometric As:Ga ratios. The models capture incorporation dynamics with some success by taking various growth processes into account, however, given the assumptions none can account for Bi droplet formation or compositional inhomogeneity. Given the ubiquity of these phenomena, these growth processes need to be more accurately captured to improve growth parameter selection.

To grow a GaAsBi or GaSbBi film with a clean surface and the desired composition, the kinetics involved need to be understood. The kinetic model presented here has similarities to those presented by Lu et al.[12] and Lewis et al[7], but is written generally for any III-V alloy containing Bi, and takes droplet formation into account. The consequence of having different group V alloy constituents on the kinetics is that the relative rates of the growth processes are different due to differing bond energies. Figure 3-4 illustrates the processes considered in the growth of bismides. Impinging Bi, given by the incoming flux F_{Bi}, may physisorb onto the surface forming a weakly bound surfactant layer. The physisorbed Bi may then chemisorb to the crystal termination layer

by forming a III-Bi bond. Alternatively, Bi in the surfactant layer may either desorb, or be ejected by an incoming group V atom. While in the crystalline layer, the Bi can undergo anion exchange[13] with an incoming group V atom, returning the Bi to the surfactant layer. Equations for the accumulation of each species can be written in terms of these processes.

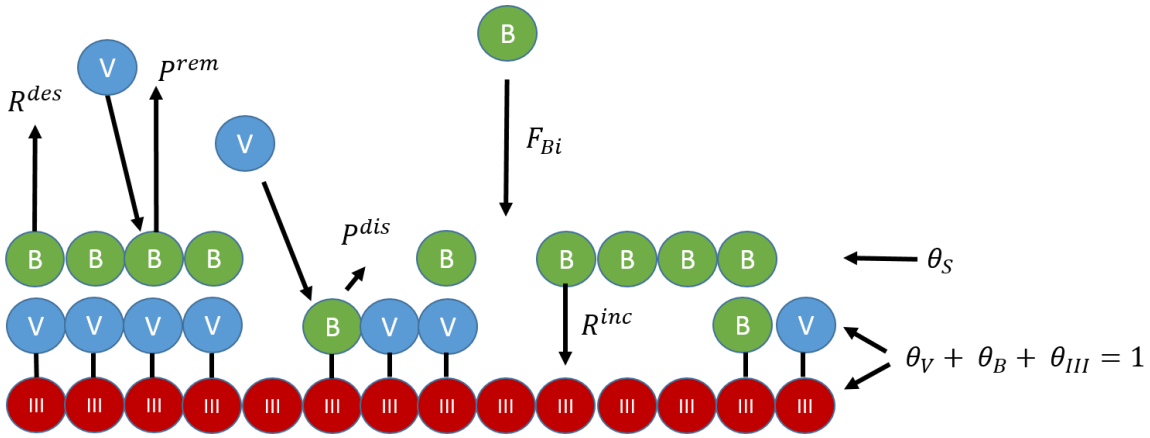

Figure 3-4: Illustration of possible operating mechanisms during the deposition of Bi in the growth of III-V-Bi. [14]

The surfactant layer will be kept track of in the following manner; the total number of Bi atoms in the surfactant layer is denoted as S (in units of fractional monolayers) and the fraction of the surface it covers is θ_S. It is assumed that the surfactant layer will completely fill the first layer before becoming multiple atoms thick, meaning $\theta_S = S$ when $S \leq 1$, and $\theta_S = 1$ when $S > 1$. It is also assumed that all processes relating to the surfactant layer only occur on the topmost or bottommost layer, all sticking coefficients are unity, and there are no droplets on the initial surface. The (001) crystal orientation is considered as that is the preferred experimental substrate orientation, providing restrictions for the crystalline layer. The surfactant layer will have the same interactions regardless of crystalline orientation and is not tracked. From here the time rate of change of *S*, can be written as follows:

$$\frac{dS}{dt} = F_{Bi} - \theta_S R^{des} - \frac{\theta_{III}\theta_S R^{inc^2}}{F_V} + \theta_B F_V P^{dis} - F_V \theta_S P^{rem} \qquad (1)$$

The first term, F_{Bi}, is the flux of arriving Bi. The second term accounts for the reduction in the surfactant coverage due to desorption, which occurs at a rate R^{des} and is scaled by the surface coverage of the surfactant layer, θ_S. The third term accounts for Bi incorporation into the crystal termination layer by forming a III-Bi bond, which occurs at a rate R^{inc}. This term is scaled by the product of the group III site coverage in the crystal termination layer θ_{III} and the surfactant coverage. It is limited by the competition for the group III sites by the group V and Bi atoms. Assuming that the arrival rate of the group V atoms, F_V, is much faster than the incorporation of Bi, that scaling term is $\frac{R^{inc}}{F_V}$. Both R^{des} and R^{inc} depend on an activation energy for each process and the temperature T in the standard Arrhenius form, $\exp(\frac{E_a}{kT})$. The fourth term takes anion exchange, the tendency for the other group V element to displace Bi from the crystal termination layer to the surfactant layer, into account. This process is associated with the probability P^{dis}, and is scaled by the Bi coverage θ_{Bi} and F_V. The final term considers a process in which the incoming group V element can eject Bi from the surfactant layer with probability P^{rem}, and is scaled by the product of F_V and θ_S. These probabilities have a similar Arrhenius behavior when compared to R^{des} and R^{inc}.

Similarly, the rate equation for θ_{III} is:

$$\frac{d\theta_{III}}{dt} = (\theta_V + \theta_B)F_G - \frac{\theta_{III}\theta_S R^{inc^2}}{F_V} - \theta_{III}F_V \qquad (2)$$

Here the first term is the creation of a Ga site from Ga impinging on the surface and forming a bond with a group V or Bi atom. Ga sites may be removed by Bi incorporation, accounted for by the second term, or by group V chemisorption, accounted for by the third term. Finally, the rate equation for Bi sites in the crystal termination layer is:

$$\frac{d\theta_B}{dt} = \frac{\theta_S \theta_{III} R^{inc^2}}{F_V} - \theta_B F_V P^{dis} - \theta_B F_{III} \qquad (3)$$

Where Bi sites are created by Bi incorporation from the surfactant layer (the first term), and removed by Bi displacement back into the surfactant layer (the second term), or covered by incoming group III atoms (the third term).

This system of equations has a large number of interacting processes, many of which are not well characterized. Several assumptions need to be made to obtain tractable solutions. Recent reports indicate that the incorporation percentage of Bi, x, is small when there are no droplets on the surface[7]. Thus, higher order effects on incorporation such as clustering and/or ordering are neglected. Given that $x=\theta_B/(\theta_B+\theta_V)$, θ_B must also be small. Because in steady state θ_B is proportional to $\frac{\theta_S \theta_{III} R^{inc^2}}{F_V}$ according to eq. 3, $\frac{\theta_S \theta_{III} R^{inc^2}}{F_V}$ must also be small relative to other terms present in eq. 1. Thus, the third and fourth terms in eq. 1 are neglected such that in steady state ($\frac{d\theta_S}{dt} = 0$):

$$S = \theta_S = \frac{F_B}{R^{des} + F_V P^{rem}} \quad for \;\; S \leq 1 \; (4)$$

From this equation, the minimum Bi flux necessary to support $S = \theta_S = 1$ is equal to the sum of the desorption and removal terms.

This resulting form for *S* closely resembles a Langmuir isotherm with two differences. The first is the addition of the process by which Bi atoms in the surfactant layer are removed by impinging group V atoms in our initial formulation. The second is the absence of a self-limiting term in the denominator. The Langmuir isotherm assumes that S reaches a single monolayer of coverage, and no more. However, the formation of droplets demonstrates that *S* can exceed unity. To account for this buildup, our model allows all incoming Bi to adsorb on any type of site.

Next, we consider the case where the Bi flux is large enough for $S > 1$. In this flux regime the effective coverage of Bi in the surfactant layer is unity ($\theta_S = 1$) even if the total number of Bi atoms in the surfactant layer, S, is greater than one monolayer. Thus, the negative terms in equation 1 are constant, and cannot compensate for increasing F_B, resulting in a net increase in S with time. This is the driving force for droplet formation, which can be described by an excess flux, F_{xs}:

$$F_{xs} = F_{Bi} - R^{des} - F_V P^{rem} \qquad (5)$$

the difference between F_B (the numerator in eq. 4) and the sum of the desorption and removal terms (the denominator in eq. 4). Nucleation of Bi droplets occurs after some nucleation time once a critical S value is reached. As the nucleation process continues, surface Bi is consumed reducing the surfactant coverage, and necessitating the reappearance of the θ_S :

$$\frac{dS}{dt} = F_{Bi} - \theta_S R^{des} - \frac{\theta_{III}\theta_S R^{inc^2}}{F_V} + \theta_B F_V P^{dis} - F_V \theta_S P^{rem} - \theta_d(t) R^{dr} \qquad (6)$$

where the term, $\theta_d R^{dr}$, is the rate of Bi uptake into the droplets scaled by the areal coverage of the droplet θ_d. For simplicity, R^{dr} is assumed to be large and effectively constant as a function of

droplet size. The amount of Bi in the droplets varies monotonically with the amount of deposited Bi, such that θ_d scales with time. Here it is assumed that the Bi atoms in the droplets are inactive participants in the crystal growth, and the transition between growth without droplets (where there is a steadily growing surfactant layer), and growth with droplets (where there are steadily growing droplets) is short. The approximate value of S in this latter regime is:

$$S(t) = \frac{F_B - \theta_d(t)R^{dr}}{R^{des} + F_V P^{rem}} \quad (7)$$

3.5 Implications and Experimental Verification of Model

Trends can now be identified from the model and compared to the current set of known results. The first trend to analyze is how the total Bi incorporation varies as a function of growth conditions, such as growth rate. Assuming there are no droplets on the surface, the steady state values of θ_B and θ_{III} may be solved using eqn. 2 and 3. The Bi incorporation x is given by the ratio of the θ_B to 1-θ_{III}:

$$x = \frac{F_{III}R^{inc^2}F_B}{(F_{III} + F_V P^{dis})(F_V^3 P^{rem} + F_V^2 R^{des} + R^{inc^2}F_B)} \quad (8)$$

Figure 3-5 is a plot of the expected incorporation, x, across a range of F_{III} and F_{Bi} with constants of R^{inc} = 0.015; $\frac{F_V}{F_{III}}$ = 1; P^{dis} = .1; P^{rem} = .1; R^{des} = .1. The values for each of the rates are not known, but experimental data suggests that R^{inc} should be significantly smaller than the others. As expected, x increases with increasing F_B. Furthermore, as F_{III} increases while holding the F_V/F_{III} ratio constant, x is lower for a given value of F_B. This is because increasing F_{III} and thus F_V, reduces θ_S (eq 4). As a result, equivalent Bi incorporation at higher Ga flux with constant V:III ratio requires higher values of F_{Bi}, in agreement with reports by Ptak et al. Equation 8 is

only valid in the absence of droplets, or when F_{xs}<=0. When F_{xs}>0, droplets may form due to excess Bi on the surface. The conditions for F_{xs}=0, or the critical flux for droplet formation F_{crit}, are also indicated in Fig. 3-5.

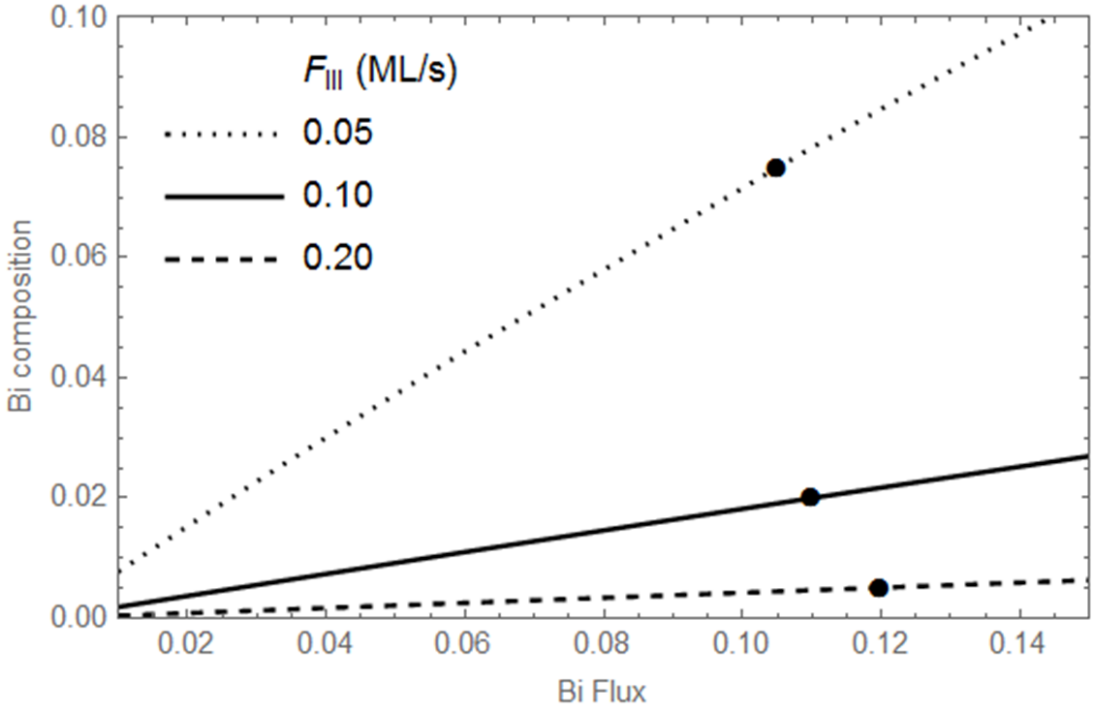

Figure 3-5: Bi composition as a function of Bi flux (ML/s), F_{Bi}, for various group III fluxes using the kinetic model with R^{inc} = 0.015; $\frac{F_V}{F_{III}}$ = 1.0; P^{dis} = 0.1; P^{rem} = 0.1; R^{des} = 0.1. Filled circles represent the maximum F_{Bi} before droplet formation. [14]

Experimental findings of Lu et al show that increasing the growth temperature from 270°C to 360°C reduces the incorporation, thus requiring higher Bi:V flux ratios to achieve similar compositions[12]. Because all rates are assumed to be Arrhenius and thus increase with increasing temperature yet not all activation energies are known, the changes in rates with respect to temperature are unknown. Nonetheless, inspection of eq. 8 suggests that R^{inc} must change more slowly than the other rates in order to observe the reduction in composition with

increasing temperature. Activation energies for some of these processes, namely desorption[15] has been reported.

With the incorporation as a function of growth conditions matching reported trends in the absence of droplet formation, the predictions of the model in the regime where droplets do form can now be examined. F_{xs} >0 drives droplet formation, and therefore directly results in an increase in areal droplet coverage θ_D . θ_D is proportional to the number of excess Bi on the surface, given by the product $F_{xs} * t$. Because the experiments had the same amount of deposited material and were grown under group III limited conditions, the time t is inversely proportional to F_{III}. Thus θ_D is proportional to F_{xs}/F_{III} and

$$\theta_D = \frac{F_{xs}}{F_{III}} = \frac{F_{Bi} - R^{des} - F_V P^{rem}}{F_{III}} \qquad (9)$$

Equation 9 can now be used as a metric to analyze the trends expected from the model to the droplet coverage observed in growth experiments.

GaSbBi films were grown on GaSb(001) substrates by molecular beam epitaxy (MBE). All substrates then had a ~30nm GaSb buffer layer grown at ~485°C. 500nm GaSbBi films were grown at 305°C using conditions listed in Table 3-1.

Sample #	Ga Rate (ML/s)	Sb:Ga	Bi:Ga	Sb:Bi	θ_d
1	0.50	1.66	0.82	2.04	.34
2	0.50	1.66	0.42	3.99	.24
3	0.10	1.34	0.79	1.70	.08
4	0.10	1.86	0.49	3.83	.02(pits)
5	0.10	3.21	0.92	3.47	.01
6	0.56	1.00	0.83	1.21	-

Table 3-1: Table of Ga growth rate (ML/s), and BEP flux ratios for the samples examined in this paper, along with resulting droplet coverages (if measured).

According to eq. 9, increasing F_{Bi} results in an increase in θ_d holding all other parameters constant. Figure 3-6 shows SEM images of GaSbBi samples grown at T=305°C, F_V/F_{III}≈1.66, using combinations of F_{III}= 0.5 ML/s and 0.1 ML/s and F_{Bi}/F_{III}= 0.8 and 0.5. As expected, the droplet coverage increases with increasing F_{Bi}. Fig. 3-6 illustrates the differences in droplet coverages by changing F_{III} while keeping all flux ratios equal and comparing image pairs top to bottom shows the differences in droplet coverage when increasing F_{Bi}. Increasing droplet coverage with increasing F_{Bi} were also reported in GaAsBi[8,9]. In Fig. 3-6b there are pits observed on the surface instead of droplets. We presume that the pits seen in Fig 3-6 are remnants of Bi droplets that desorbed away during the final annealing step[10,16]. A more interesting prediction of the model is θ_D as a function of F_{III}. As before, θ_D is predicted to increase with increasing flux but saturates at high F_{III} due to the diminishing impact of the desorption term (Fig. 3-6e). By increasing F_{III} but keeping the flux ratios equivalent means that the only term changing in eqn. 10 is R^{des}/F_{III}. Increasing F_{III} holding all other parameters constant causes a significant change in droplet coverage. θ_D increases from 8% to 34% for

samples with high Bi:Ga (3 and 1 in Table 3-1) ratio and 2% of a pitted surface and 24% droplet coverage for samples with a low Bi:Ga(4 and 2 in Table 3-1). This experimental result paired with our model suggests that growing at lower F_{III} suppresses droplet formation.

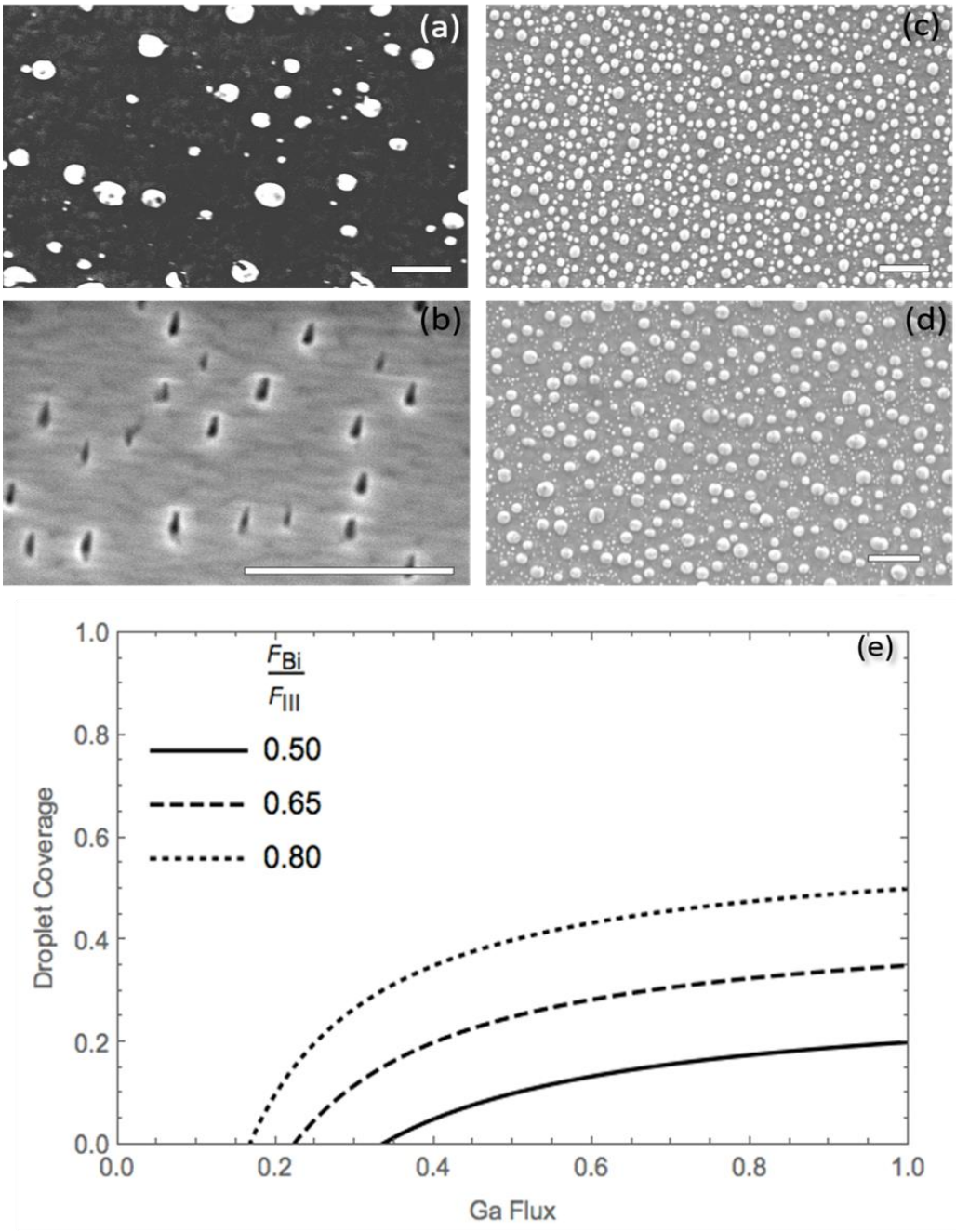

Figure 3-6: SEM images of GaSbBi films (sample 3(a), 4(b), 1(c), and 2(d)) grown at different group III rates and Bi:Ga BEP ratios. Scale bars in each image represents 5µm. (e) Predicted droplet coverage as a function of group III growth rate and Bi:Ga flux ratio.[14]

The model suggests that the removal of Bi from the surfactant layer by impinging group V strongly impacts both the incorporation of Bi (eq. 8) and the formation of droplets (eq. 10). The removal term can be experimentally isolated by changing the Sb flux while keeping the other growth conditions constant. Sample 3 has 8% droplet coverage under lower Sb conditions and sample 5 has ~1% coverage under higher Sb conditions as can be seen in Fig. 3-7. This result confirms the necessity of the inclusion of the removal term for the kinetic expressions and suggests that V-rich conditions reduces the droplet coverage and Bi composition. The results in GaSbBi and the prediction of the model are also consistent with observations by by Ptak et al. for GaAsBi. In that work, higher F_{Bi} were required required for droplet formation as F_{Ga} and F_{As} increased[9].

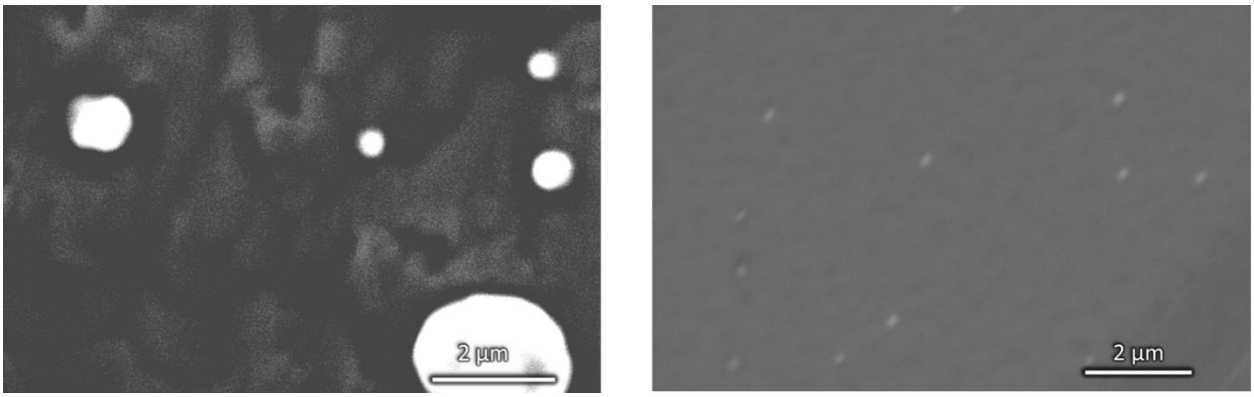

Figure 3-7: SEM images of GaSbBi films grown at T=305C, F_{III}= 0.1ML/s , with Sb:Bi = 1.7 Bi:Ga=0.79 (left, sample 3) and Sb:Bi = 3.47 Bi:Ga=0.92(right, sample 5).[14]

Temperature plays an important role in all of these equations. A change in temperature would change the incorporation and desorption rates, as well as adjust the probability of removal and displacement. However, the absolute values of each is not well characterized. Furthermore, their impact on experimentally observable properties, composition in particular, is complex as seen in eq. 8. A possible route to overcome this challenge is suggested in eq. 9. Here, we see that an increase in temperature, which would increase R^{des} and P^{rem} , would reduce the droplet

coverage. Thus, the model provides a strategy to isolate the activation energies of some of these terms.

Droplet nucleation reduces the number of Bi atoms in the surfactant layer (eq. 7), and thus reduces θ_B. The result is that the Bi incorporation is also reduced according to the expression:

$$x = \frac{F_{III}R^{inc^2}(F_B - \theta_d R^{dr})}{(F_{III}+F_V P^{dis})(F_V^3 P^{rem}+F_V^2 R^{des}+R^{inc^2}(F_B-\theta_d R^{dr}))} \quad (10)$$

The only difference between this equation and eq. 8 is the subtraction of $\theta_d R^{dr}$ from all F_B terms. Thus, the Bi incorporation decreases when droplets nucleate on the surface, despite the fact that all other growth conditions remain constant. As a result, there is a high composition near the film-substrate interface that decreases with increasing thickness as droplets form on the surface.

Our samples also show that there is a change in composition over the thickness of the film. Figure 3-8 shows XRD of sample 6 that has been fit with Gaussian lineshapes demonstrating a clean fitted with a substrate peak and two film peaks. These three distinct peaks correlate to the substrate peak, a low Bi composition film peak, and a broader less intense high Bi composition film peak. Though the sequence of these two layers cannot be deduced from XRD alone, similar compositional inhomogeneity was observed in GaAsBi where there was an initial high concentration near the substrate that decreased with increasing thickness[1]. This compositional variation was also predicted by kinetic Monte Carlo (KMC) simulations calibrated for GaAsBi[17]. In these simulations a droplet free growth had constant Bi composition throughout the thickness of the film, and the case where a Bi droplet nucleates the composition behaves just

as predicted in the kinetic model with high initial Bi incorporation and then reduced upon Bi droplet formation. This also agrees with what is found experimentally in the above section.

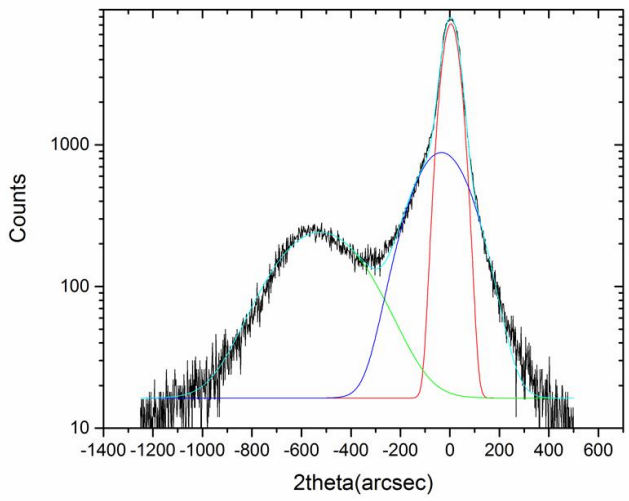

Figure 3-8: XRD data for a GaSbBi film grown at T=305°C, F_{III}=0.56ML/s, Bi:Ga=0.83, Sb:Ga=1.0 (sample 6). The dotted lines represent Gaussian fits to (from right to left) the GaSb(001) substrate peak, an x~1% $GaSb_{1-x}Bi_x$ film peak, and an x=~5% $GaSb_{1-x}Bi_x$ film peak.[14]

It should be noted that there might be an additional explanation for the observed compositional inhomogeneity that relies on strain-limited incorporation. For instance, rather than the nucleation of strain–relieving 3D islands, it may be possible for the Bi to be ejected from the crystalline layer back to the surfactant layer as the strain-energy of the film approaches the critical thickness. This effect would increase the surfactant concentration, driving droplet formation and limiting incorporation as well.

3.7 Summary

This chapter covered the initial approach to optimizing Bi incorporation in III-V-Bi alloys. The initial target via surface reconstructions is shown to be flawed due to the double anion layer in the reconstructions targeted. A kinetic model is built as an extension of previously postulated models set to include the accumulation of Bi on the surface. The model is corroborated by growth experiments of GaSbBi films by showing the difference of Bi droplet coverage under a variety of conditions. Bi droplets are postulated to become a kinetic sink for impingent Bi leading to a reduction of the Bi incorporated in the film once droplets have nucleated. The different film compositions are found in both experiments and KMC simulations. The experiments and model in this chapter rules out growths that have Bi droplets due to the consequence of inhomogeneous Bi distribution. The next chapter sets to explore the inhomogeneities that exist from Ga droplets and growth temperature dependent inhomogeneities.

3.8 References

1. Reyes, D. F. *et al.* Bismuth incorporation and the role of ordering in GaAsBi/GaAs structures. *Nanoscale Res. Lett.* **9,** 23 (2014).
2. Mohmad, a R. *et al.* Bismuth concentration inhomogeneity in GaAsBi bulk and quantum well structures. *Semicond. Sci. Technol.* **30,** 94018 (2015).
3. Janotti, a., Wei, S.-H. & Zhang, S. Theoretical study of the effects of isovalent coalloying of Bi and N in GaAs. *Phys. Rev. B* **65,** 115203 (2002).
4. Duzik, A. & Millunchick, J. M. Surface reconstruction stability of Bi/GaSb surfaces. *J. Appl. Phys.* **116,** 1–5 (2014).
5. Duzik, A., Thomas, J. C., Van Der Ven, A. & Millunchick, J. M. Surface reconstruction stability and configurational disorder on Bi-terminated GaAs(001). *Phys. Rev. B - Condens. Matter Mater. Phys.* **87,** 1–9 (2013).
6. Duzik, A. *et al.* Surface structure of bismuth terminated GaAs surfaces grown with molecular beam epitaxy. *Surf. Sci.* **606,** 1203–1207 (2012).
7. Lewis, R. B., Masnadi-Shirazi, M. & Tiedje, T. Growth of high Bi concentration GaAs1−xBix by molecular beam epitaxy. *Appl. Phys. Lett.* **101,** 82112 (2012).
8. Vardar, G. *et al.* Mechanisms of droplet formation and Bi incorporation during molecular beam epitaxy of GaAsBi. *Appl. Phys. Lett.* **102,** 42106 (2013).

9. Ptak, A. J. *et al.* Kinetically limited growth of GaAsBi by molecular-beam epitaxy. *J. Cryst. Growth* **338,** 107–110 (2012).

10. Duzik, A. & Millunchick, J. M. Surface morphology and Bi incorporation in GaSbBi(As)/GaSb films. *J. Cryst. Growth* **390,** 5–11 (2014).

11. Rajpalke, M. K. *et al.* Growth and properties of GaSbBi alloys. *Appl. Phys. Lett.* **103,** 142106 (2013).

12. Lu, X., Beaton, D. a., Lewis, R. B., Tiedje, T. & Whitwick, M. B. Effect of molecular beam epitaxy growth conditions on the Bi content of GaAs[sub 1−x]Bi[sub x]. *Appl. Phys. Lett.* **92,** 192110 (2008).

13. Brown, A. S., Losurdo, M., Bruno, G., Brown, T. & May, G. Fundamental reactions controlling anion exchange during the synthesis of Sb/As mixed-anion heterojunctions. *J. Vac. Sci. Technol. B Microelectron. Nanom. Struct.* **22,** 2244 (2004).

14. Tait, C. R. & Millunchick, J. M. Kinetics of droplet formation and Bi incorporation in GaSbBi alloys. *J. Appl. Phys.* **119,** (2016).

15. Young, E. C., Tixier, S. & Tiedje, T. Bismuth surfactant growth of the dilute nitride GaNxAs1−x. *J. Cryst. Growth* **279,** 316–320 (2005).

16. Moussa, I. Effect of thermal annealing on structural and optical properties of the. **125034,** 24–28

17. Rodriguez, G. V. & Millunchick, J. M. Predictive modeling of low solubility semiconductor alloys. *J. Appl. Phys.* **120,** (2016).

Chapter 4: Inhomogeneities in III-V-Bi Alloys

4.1 Introduction

Maximal Bi incorporation is shown occur at high Bi fluxes and low relative group V fluxes. The previous chapter saw that excessive Bi in growths nucleate into droplets and can lead to step function-like inhomogeneity through the thickness of the film. Rodriguez et al. built up a surface morphology phase diagram using kinetic Monte Carlo simulations[1]. Their work reveals a small parameter window in which there is high Bi incorporation with no surface droplets. The highest Bi incorporation leads to the droplet formation regions. It is critical to know if any of the droplet formation regions provide homogeneous Bi distribution making it a more useful electronic material candidate.

Compositional inhomogeneities in III-V semiconductor alloys are crucial to understand, as such fluctuations can cause carrier localization[2] and degradation of device performance. They are often driven by thermodynamics, resulting in phase separation or ordering. Many alloys are predicted to have miscibility gaps, including InGaN[3], InAsSb[4], and InAsBi[5]. Other materials show a propensity for atomic ordering, such as InGaP[6] and GaAsBi[7], but those effects are thought to be related to the surface reconstructions present during growth. Kinetic effects also lead to compositional inhomogeneities. For example, lateral compositional modulations were observed arising from the interaction of atomic mismatch with morphological undulations[8]. Compositional variation along the growth direction due to surface segregation was also observed[9], as has compositional variation near dislocations[10].

In the previous chapter we saw that nucleation of Bi droplets could lead to reduced Bi incorporation creating inhomogeneous incorporation through the thickness of the film. This chapter sets to explore other compositional inhomogeneities that are encountered in III-V-Bi films. Ga droplets are shown to generate a Bi composition inhomogeneity and growths with clean surface are also shown to have conditions in which the Bi is not homogenous.

4.2 Experimental Methods

All films in this chapter were still grown with MBE and characterized with XRD and SEM as described in the previous chapter. In addition to these methods, the films Bi distribution in the bulk was characterized by atom probe tomography (APT) and scanning transmission electron microscopy (STEM). Both techniques allow for high resolution insight into how Bi is distributed in grown films.

4.2.1 Nanometer Scale Structural and Compositional Characterization

Samples that were examined with scanning tunneling electron microscopy (STEM) using a JEOL JEM 2100 Scanning transmission electron microscope. All images were taken in high angle annular dark field (HAADF) mode. In this image scheme the pixel intensity is measured by an annular detector representing high angle scattering from the incident electron beam direction. The scattering cross section for high angles is highly dependent on the atoms core charge z and is commonly referred to as “z contrast” imaging. For GaAsBi, this leads to stark contrast between As and Bi allowing for identification of how Bi is distributed in the samples with the high resolution provided by STEM. GaSbBi was much harder to get contrast on low composition films, so there is no analysis of those films within this dissertation. The GaAsBi samples were prepared via focused ion beam (FIB) lift out. For any work involving GaSb it is necessary to create samples using mechanical polishing since FIB is not viable due to material redeposition.

Samples that were examined with STEM were also characterized via atom probe tomography (APT) with a Cameca LEAP-4000HR. APT is a relatively new technique where a small tip of the sample is set at a bias voltage and excited with a pulsed high energy electric field, ejecting atoms in an individually measurable fashion. The ejected atoms are measured with positional time of flight mass spectrometry for atom position and atomic mass determination. A reconstruction of the tip can then be made and is the subject of the analysis done throughout this chapter. The tips are also prepared via FIB lift out methods. More details of these two characterization techniques and sample preparation can be found in Lifan Yan's thesis[37], who prepared the samples and performed the measurements.

4.3 Ga Droplet Induced Inhomogeneities

As seen from the previous chapter, the fluxes of each element must be carefully optimized to eliminate the formation of Group III and/or Bi droplets while simultaneously maximizing the amount of Bi incorporation. The KMC work discussed previously by Rodriguez[1] showed that the highest Bi incorporation rates are predicted in the flux regime where Ga droplets form but Bi droplets do not. This is because Bi incorporation requires a high coverage of available Ga sites. Once Bi droplets form, Bi incorporation into the film is no longer thermodynamically favorable, and can result in a compositional inhomogeneity along the growth direction[7].

Despite the fact that the highest Bi incorporation is predicted to occur in the presence of Ga droplets, it is generally desirable to grow in a regime without them because they tend to roughen the surface[11]. This section investigates the impact Ga droplets at the growth front have on the crystal quality of GaAsBi films. It is found that the appearance of Ga droplets correlates with nanometer-sized compositional fluctuations across the entire film thickness, which we

propose arises due to local variations in the Bi incorporation at the growth front as a result of nonuniform Ga flux in the vicinity of the droplets.

Samples began with the deposition of a 250nm-thick GaAs buffer layer at 600°C. Then 500 nm-thick GaAsBi films were grown at 315°C, a Ga growth rate of 0.97 ML/s, and a Bi beam equivalent pressure (BEP) of 1.0×10^{-7} torr. Two samples were grown as continuous films: one with an As:Ga BEP ratio of 3.5 (expected flux ratio of 1.1), and one with a ratio of 1.7 (expected flux ratio of ~0.6). Two additional samples were grown at BEP ratios of 1.7, except that they were grown with periodic interruptions of the Ga and Bi fluxes while maintaining the As flux. One sample was interrupted every 50nm of deposited thickness, and the other was interrupted every 25nm. The interruptions lasted half the time it took to grow the relevant thickness (i.e. 1 min film growth followed by 30 sec interruption) in order to keep the total As exposure the same for both samples. Thus, the effective As to Ga ratio was 2.55 for both interrupted samples.

Maximizing Bi incorporation in a GaAsBi film at a given Bi flux and growth temperature is an important feature to understand. Kinetic models and prior experimental work suggest that the optimal incorporation occurs when the growth front is Ga-rich[12–14]. If precise stoichiometric conditions aren't met for the ratio of As and Ga fluxes, Ga atoms accumulate on the surface forming droplets. This effect can be seen in Fig. 4-1, which shows a comparison of scanning electron microscopy (SEM) images for films grown continuously with a As to Ga BEP ratio of 1.7 and 3.5. The film grown with a BEP ratio of 1.7 has a distribution of droplets ranging in diameters up to 10 μm. These droplets are comprised of Ga, according to energy dispersive spectroscopy (EDS) [not shown], confirming an As deficiency. The film grown at a BEP ratio of 3.5 has a surface devoid of droplets, suggesting that the stoichiometric requirement for growth, that is a one to one ratio of group III and group V atoms, are met.

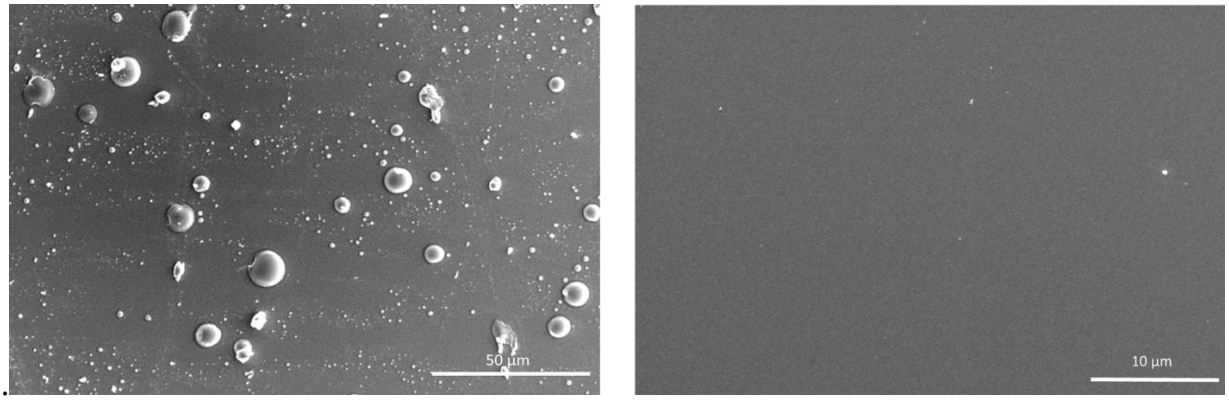

Figure 4-1: (left) SEM image of sample grown at As:Ga BEP=1.7 revealing large Ga droplets distributed across the surface; (right) SEM image of sample grown at As:Ga BEP=3.5 showing a relatively clean surface.[15]

The Ga droplets on the surface of the film grown continuously at an As to Ga BEP ratio of 1.7 result from the buildup of excess Ga due to an As deficiency. Growth interrupts were used to grow films with cleaner surfaces while maintaining Ga-rich conditions to promote Bi incorporation. The purpose of the growth interrupt is to convert excess Ga on the surface into GaAs thus restricting its buildup over the course of the film growth. Figure 4-2 shows SEM images of the surface of two samples grown using an As to Ga BEP ratio of 1.7 as previously, except with growth interrupts every 50nm or 25nm of deposited GaAsBi. Overall, the Ga droplets are much smaller in both samples compared to the film without interrupts. The sample with interrupts every 50 nm exhibits a surface covered by a high density of Ga droplets with diameters on the order of 200 nm. Doubling the frequency of the interrupts to every 25nm of GaAsBi film thickness results in even smaller features, more closely resembling the surface of the continuous film grown with a As to Ga ratio of 3.5, suggesting that excess Ga is eliminated.

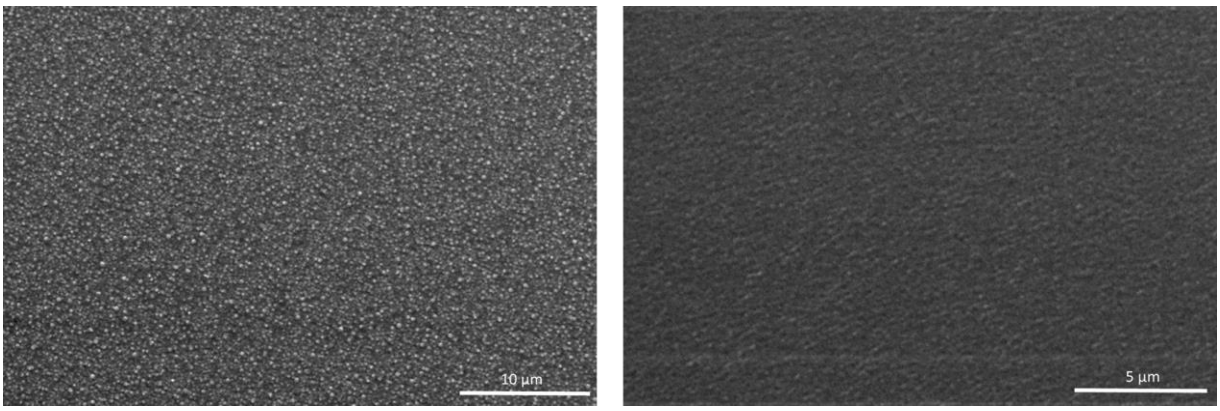

Figure 4-2: (left) SEM image of 50 nm growth interrupt film revealing many Ga droplets; (right) SEM image of 25 nm growth interrupt film showing a relatively cleaner surface with roughening similar to the other growth interrupt but on a much smaller scale.[15]

The crystal quality and average lattice parameter are strongly influenced by both the As to Ga BEP ratio and growth interrupts. Figure 4-3 shows the (004) x-ray diffraction of each of the films. The sample grown continuously with a As to Ga BEP ratio of 3.5 exhibits a film peak 568 arcsec to the left of the substrate peak corresponding to a Bi composition of ~2% assuming Vegard's law, no strain relaxation, and that the lattice parameter of GaBi is 6.33Å [16]. Furthermore, the 71 arcsec full width half maximum (FWHM) of the film peak suggests high crystal quality. The x-ray diffraction (XRD) data for the continuous film with an As to Ga BEP ratio of 1.7 exhibits no distinct film peak. Instead it appears as a broad peak indicative of a large variation in the lattice parameter of the film, perhaps due to point defects, compositional variation, or the precipitation of As clusters[17]. The two interrupted films appear to be some linear combination of the XRD of the two continuous films. The XRD data for the 50nm growth interrupt sample has a small film peak at ~2% Bi superimposed over a broad signal. The XRD data for the 25 nm interrupted film more closely resembles the continuous film grown at As to Ga of 3.5, but with a slightly broader (100 arcsec) film peak superimposed upon a broad background signal. This suggests that two different growth modes are operating, one that

generates a broad film peak under As-poor conditions, and another that results a narrower film peak in As-rich conditions.

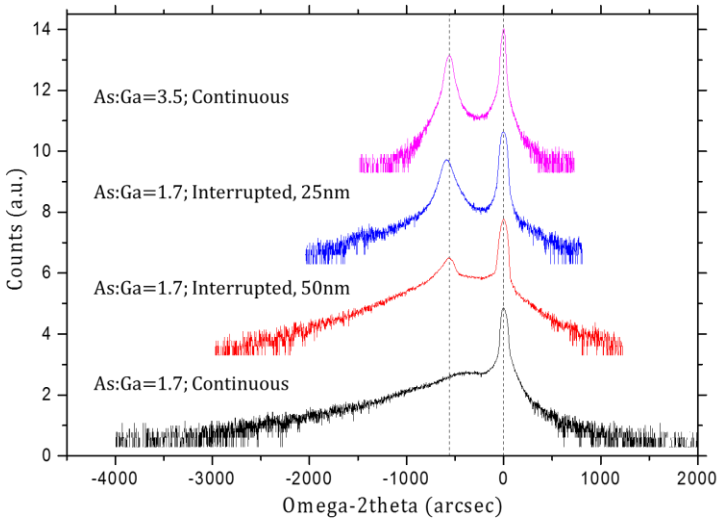

Figure 4-3: X-ray diffraction data of samples with vertical dashed lines highlighting the GaAs substrate peak at 0 arcsec and the GaAsBi film peak center on As:Ga=3.5; continuous film at 568 arcsec to highlight the appearance of the film peak in samples containing growth interrupts[15]

The differences in XRD scans and the observed SEM images together suggest that the presence of Ga droplets on the surface has a strong impact on the subsequent crystal quality of the grown film. Clearly, the appearance of droplets on the surface is correlated with a broad background signal in the XRD scans. Furthermore, it appears that the size of the droplets is inversely related to the appearance of a sharp film peak. The film grown continuously has the largest droplets on the surface and the no sharp film peak, followed by smaller droplets and a low intensity film peak for the 50nm interrupted film. The 25nm interrupted film has the smallest droplets, and the XRD scan that most resembles the high-quality film grown at high BEP. Presumably, Ga droplet nucleation results in a change in the growth conditions that either alters

the incorporation of Bi, or induces the injection of defects, either of which could lead to the observed variation in the lattice parameter.

Transmission electron microscopy (TEM) and atom probe tomography (APT) were performed to determine the origin of the broadening of the GaAsBi XRD film peaks. Figure 4-4a shows a High Angle Annular Dark Field (HAADF) TEM image of the sample grown continuously with an As to Ga BEP ratio of 1.7. The TEM data shows plate-like contrast variation across the thickness of the film, indicative of a variation in the Bi composition parallel to the growth front. The contrast variation observed in Fig. 4-4a is markedly different from previously reported composition variation in Bi-containing films. For instance, Reyes et al. report a linear gradient in Bi composition parallel to the growth direction when grown at 380°C with As_4:Ga:Bi BEP ratios of 40:2:1 [7], while Wu et al. [18]and Luna et al. [19]report that unannealed $GaAs_{0.985}Bi_{0.015}$ grown at T=220C results in lateral composition modulations aligned along the [110], perpendicular to the growth direction, having a periodicity of ~20nm. Presumably, those films were grown under group V rich conditions, as no Ga-droplets were reported. The plate-like variation of the Bi-composition is also observed in APT of the same sample (Fig. 4-4b). Figure 4-4c shows the variation in the Bi composition along the line shown in Fig. 4-4b, and reveals that the Bi composition varies between $0<x<7\%$ along the growth direction of the film. The width of these features can exceed 100 nm, but the thickness of these features ranges from $5<d<40$nm.

The plate like variation in the Bi composition is also observable in cross-sectional scanning tunneling microscopy(xSTM) shown in Fig. 4-5. The contrast in these images arise from an increase in the tunneling current from the Bi atoms. Brighter areas are indicative of higher Bi concentrations. The dark stripes in the image are cracks that likely appear due to a

poor cleave of the sample. The features sizes of the increased Bi composition regions agree with the 5<d<40nm size as observed in the APT.

The TEM, APT, and xSTM data taken together suggests that the peak broadening observed in the XRD scans (Fig. 4-3) are a result of compositional fluctuations as opposed to point defect injection. The compositions measured in the APT data are consistent with the observed variation in the lattice parameter measured by XRD. TEM images observing the compositional behavior near the Ga droplets is shown in Fig. 4-6. It shows that near the boundary of the droplets there is a region of enhanced Bi incorporation. There is clear distinction in the three images between Bi incorporation underneath the droplets and Bi incorporation near the droplets.

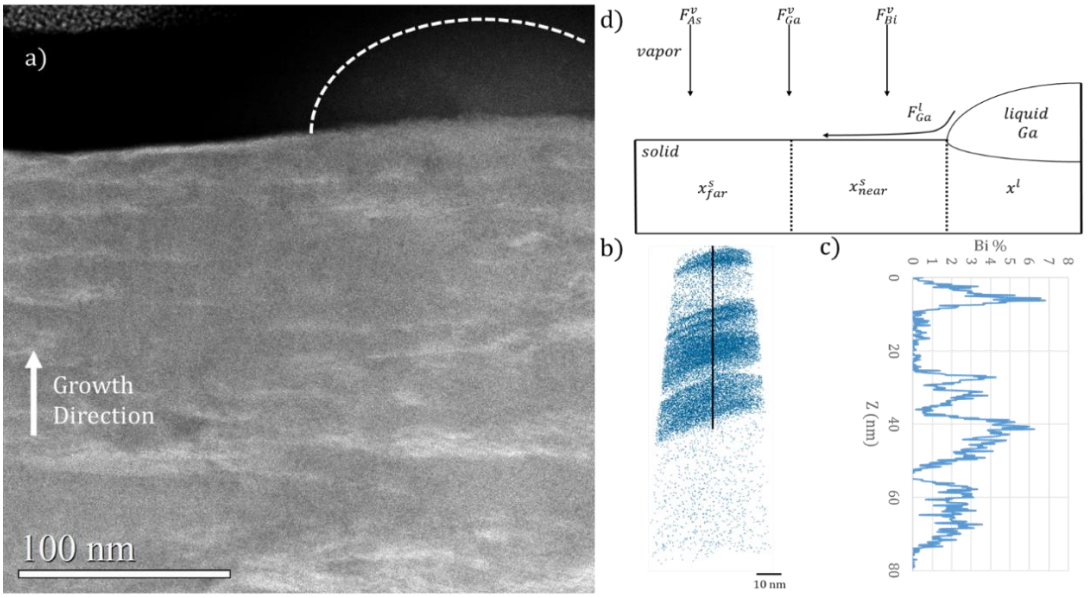

Figure 4-4: (a) High angle annular dark field image of sample grown continuously at As:Ga BEP=1.7 showing inhomogeneous distribution of Bi atoms in the film. The dotted line shows the outline for a Ga droplet on the surface; (b) Atom probe tomography of a cutout from the same sample mapping Bi atoms in blue with the vertical line representative of the top 80 nm of the sample; (c) Average Bi composition of an x-y cylindrical cross section taken along the line in part b; (d) Illustration of the available elemental fluxes and different incorporation regimes when Ga droplets are present on the growth surface[15]

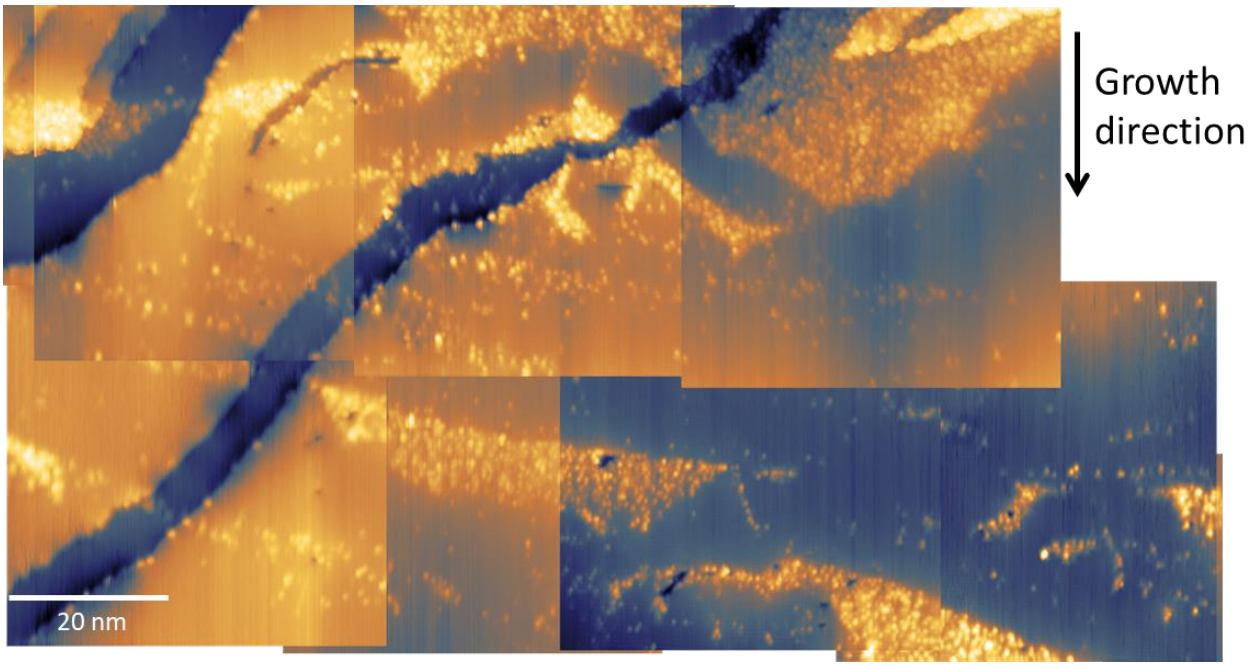

Figure 4-5: xSTM images of the continuous As:Ga BEP=1.7 film showing the variety of Bi composition. Courtesy of R.C Plantenga and P. M. Koenraad of Eindhoven University of Technology

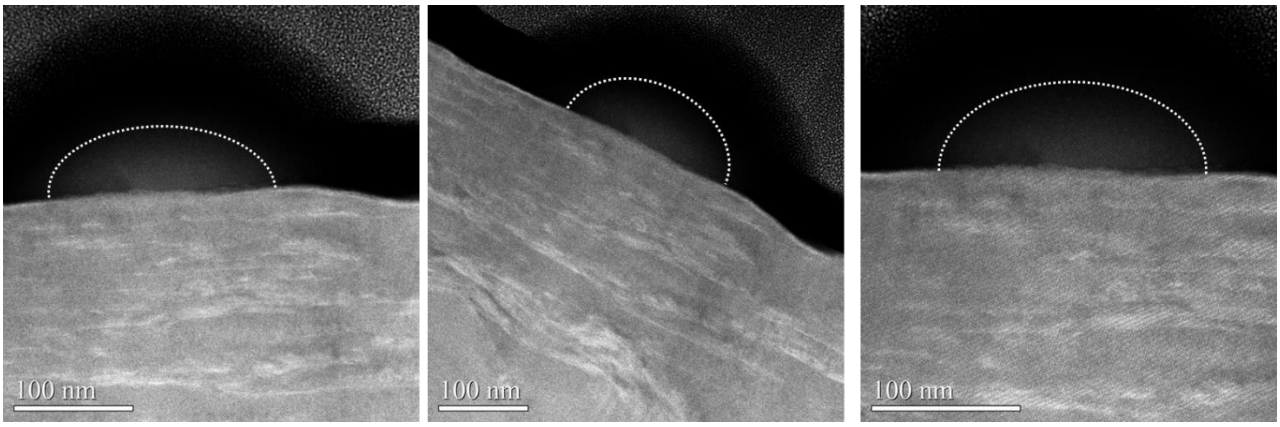

Figure 4-6: Survey of HAADF TEM images of sample grown continuously at As:Ga BEP=1.7 highlighting Bi distribution near Ga droplets.

The experimental results show that growth of GaAsBi in the presence of Ga droplets on the surface leads to Bi compositional inhomogeneity in the film. Due to the observed enhanced Bi incorporation near the droplets, the inhomogeneity is attributed to nonuniform incorporation of Bi in the presence of the droplets due to a gradient in the Ga flux. The kinetics of Bi

incorporation into MBE-grown GaAs and related materials has been examined by a number of groups,[12,14,20] and is known to depend on a number of interacting processes. In the absence of droplets, the Bi composition at the vapor-solid interface has been shown to be proportional to the Ga flux assuming constant Bi and As fluxes.[14] Typically, the source of this flux is only the flux impinging on the surface from the vapor. It is well known, however, that the Ga droplets themselves can be a source of Ga, which is the primary mechanism that allows for the observation of Group V limited RHEED oscillations.[21]Therefore, the Ga flux increases in the vicinity of the droplet, which also leads to an increase in the composition near the droplets, x^{v}_{near}, assuming that all other processes remain constant. While many of the processes are expected to be similar for the incorporation of Bi at the liquid-solid interface below the droplet, it would not be surprising if they function at different rates. Indeed, Wood et al. showed that the Bi incorporation beneath the droplets is very low.[22] Figure 4-4d shows a schematic of the impinging fluxes that result in different composition regimes: beneath the droplet, x^{l}, near the droplet, $x^{v}_{near,}$ and far from the droplet, x^{v}_{far}.

The proposed model explains the observed compositional inhomogeneities in the presence of Ga droplets. Ga droplets generate 3 regions of varying Bi incorporation that follow the Ga droplet as it moves along the surface during growth. The droplet motion would result in the plate-like variation in Bi composition as droplets move in and out of the plane where the image is taken. Other reports of GaAsBi growth under As-deficient conditions are consistent with this model. For instance, Field et al. [23] report that when the As flux is reduced to induce a Ga-terminated surface, they observe broadening of the XRD peaks, consistent with our observations and model. Similarly, Wood et al. [22] report on compositionally inhomogeneous

GaAsBi due to droplet formation, but they do not report Bi enriched regions similar to those found in our experiments. This discrepancy could arise due to the fact that those films were grown in a kinetic regime resulting in biphasic Ga-Bi droplets, which are known to be in a different kinetic regime.[1] Nonetheless, all of these experiments show that the local incorporation of Bi is enhanced by the presence of droplets on the surface, in agreement with previous predictions. [1]

While these experiments were done using an As_2 overpressure, similar results are expected under an As_4 overpressure given that the inhomogeneities occur under As-deficient conditions. The phenomenon relies on there being an excess of Ga on the surface during growth. While the stoichiometric cutoff for As_2 and As_4 are different if As availability is low enough for Ga droplets to form on the surface it is expected in this proposed mechanism for the Bi inhomogeneities to manifest.

Based on the improvement seen in the XRD data, the inhomogeneities may be ameliorated by interrupting the growth to eliminate droplets. A comparison of TEM images on the continuously grown sample vs. film grown with growth interrupts every 25 nm is shown in Fig. 4-7. The interrupted film shows overall improved Bi homogeneity in agreement with the XRD but still exhibits periodic ribbons of enhanced Bi incorporation. The intervals are a little shorter than 25nm as observable in Fig. 4-7. This is likely due to the growth being group V limited creating a growth rate slower than the deposition rate of Ga. Following from the proposed model, the small regions of enhanced Bi incorporation indicate that there is excess Ga at the surface. These regions suggests that either the interrupts were not long enough to consume all excess Ga creating enhanced Bi incorporation at the continuation of the growth or that the interrupts were not frequent enough and Ga droplets nucleate allowing for enhanced Bi

incorporation before the growth is interrupted. Based on the greatly improved homogeneity, growth interrupts are a candidate for improving the parameter space for homogeneous films by potentially allowing homogeneous growth to occur in conditions that would typically result in the Ga droplet mediated inhomogeneity discussed in this section.

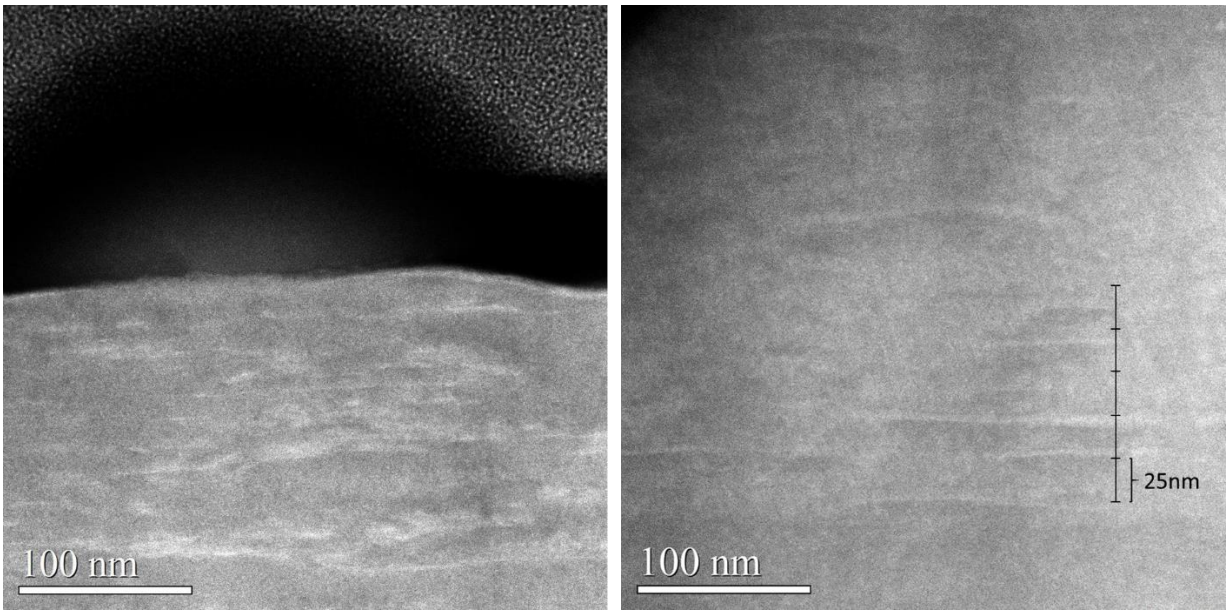

Figure 4-7: HAADF TEM images of GaAsBi grown at 315°C without growth interrupts(left) and with a growth interrupt every 25 nm (right)

Growth interrupts present an interesting direction forward. There are a few directions for optimization including interruption thickness and duration. Taking the interrupts to the limit of monolayer growth may not be the best option as it is possible Bi would not be able to incorporate and be trapped in the bulk crystal. If the enhanced Bi incorporation is occurring at the restart of growth then longer interruptions under As, or a higher As flux, would aid in consumption of the excess Ga on the surface.

4.4 Inhomogeneities in droplet free growth

It has been shown that inhomogeneities exist in every droplet formation regime for growth of GaAsBi. The question becomes whether growths of droplet free GaAsBi always result

in homogenous Bi distribution across all temperature ranges. In this section, a series of GaAsBi bulk layers were grown on GaAs (001) substrates at varying temperatures. It is shown that as the temperature decreases the composition of Bi in the film increases as expected. However many other interesting phenomena also arise with decreasing growth temperature, including lateral composition modulation, surface roughness, Bi clustering, and nanopores formation. These features appear to be correlated and are proposed to be related to a growth instabilitiy arising due to in differences in surface diffusivity between the Bi and As adatoms.

All growths began with the deposition of a 250nm-thick GaAs buffer layer deposited at 600°C, a Ga growth rate of 0.97 ML/s, and an As to Ga BEP ratio of ~3.5, which is expected to result in a ratio of 1.1 As atoms for every 1 Ga atom at the surface. Next, a series of 500 nm-thick GaAsBi films were deposited at a Bi beam equivalent pressure (BEP) of 1.0×10^{-7} torr, and substrate temperatures varying between 315°C and 350°C. These sets of growth conditions result in droplet-free growth over each of the temperatures studied. The surfaces of the films were further characterized using Atomic Force Mircroscopy (AFM) in tapping mode. The results of multiple 25 x 25 μm^2 AFM scans show that the surfaces are generally flat with the Root Mean Squared (RMS) roughness ranging from 0.8 to 2.7 nm with decreasing substrate temperature (Table 1). This finding is not surprising because as the growth temperature decreases the diffusivity of adatoms also decreases, resulting in rougher films. The average Bi composition was inferred from (004) x-ray diffraction scans assuming the lattice parameter obeys of Vegard's law and the lattice constant for GaBi is 6.33 Å [16]. These measurements indicate that the Bi composition decreases slightly from ~2% to ~1% with increasing temperature (Table 4-1), consistent with increased Bi desorption with increasing temperature [12,13].

T_g (°C)	x^{xrd}	x^{apt}	RMS^{AFM}
315	2.0%	2%	2.7 nm
325	2.2%	3%	1.3 nm
340	1.5%	2%	0.8 nm
350	1%	-	1.1nm

Table 4-1: Tabulated data of the GaAsBi films grown in this study including temperature, T_g, composition from XRD, x^{xrd}, composition from APT, x^{apt}, and RMS surface roughness from AFM.

The Bi distribution of the GaAsBi sample grown at 340°C is homogenous with few defects present. The cross-sectional HAADF TEM image in Fig. 4-8a is essentially featureless, with a slight contrast variation in the direction parallel to the growth direction. It is possible that this contrast modulation is due to a "curtaining" artifact arising from the preparation of the sample.[24]The surface appears smooth in Fig. 4-8a, in agreement with the AFM measurements. The APT reconstruction shown in Fig. 4-8b and the corresponding line profile in Fig. 4-8c corroborate both the composition of film obtained from the XRD data (see Table 4-1), and that the Bi distribution is very homogeneous. The homogeneity of the film may be quantified using the Pearson coefficient[25], which is the linear correlation between the experimental distribution and a binomial distribution centered on the average composition. Possible values range from 0, indicating a random alloy, and 1, indicating a clustered distribution of the alloy constituents. The

measured Pearson coefficient for the sample grown at 340 °C is 0.02, indicating a nominally random Bi distribution for this sample.

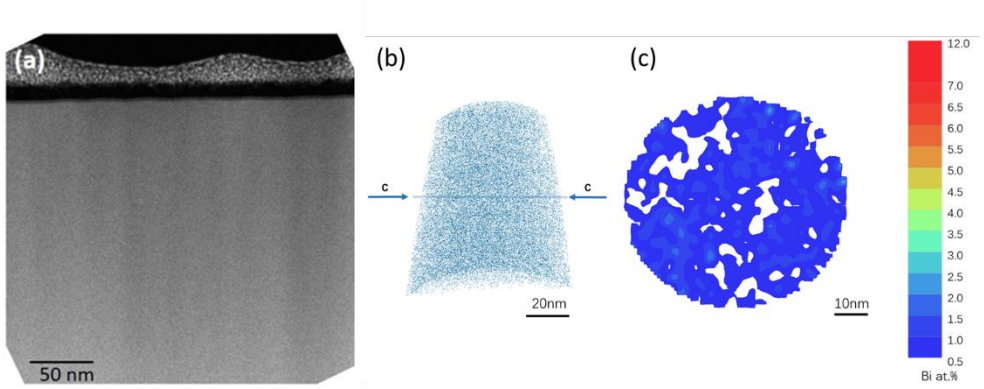

Figure 4-8: (a) HAADF TEM image of GaAsBi film grown at 340C showing some relatively even contrast; (b) APT reconstruction of the Bi distribution in the film grown at 340C; (c) Bi isoconcentration plots of a slice along a direction of the tip from (b) showing even distribution of Bi

Reducing the growth temperature to 325°C results in an increase in Bi composition, as expected due to reduced desorption[12]. The cross-sectional HAADF TEM image in Fig. 4-9a suggests that this surface is significantly rougher than the 340°C sample, in agreement with the AFM data from Table 4-1. There is also some lateral contrast variation, as in Fig. 4-9a. High resolution images show that there are distinct regions that are darker (boxed in Fig. 4-9b) that correspond to voids in the material. Brighter regions are also visible nearby, which suggests that they are enriched in Bi. The APT reconstruction volume (Fig. 4-10a) and the planar isoconcentration slices (Figs. 4-10 b and c) also exhibit a variation in the composition, with the average composition ~3% Bi, the modulation magnitude ±0.4%, and the modulation period ~25 nm. While the APT sample volume is too small to definitively determine the modulation period for the entire film, the data in Figs. 4-10a-c is consistent with the period of the contrast

modulation seen in the TEM micrograph in Fig. 4-10a. The Pearson coefficient for this sample is 0.3, consistent with a less random Bi distribution. The isoconcentration slice shown in Fig. 4-10b also exhibits a single Bi cluster with a diameter of ~3 nm having a Bi composition of up to 14% localized within a region denuded of Bi. The size of this Bi cluster is comparable to the feature observed in Fig. 4-9b.

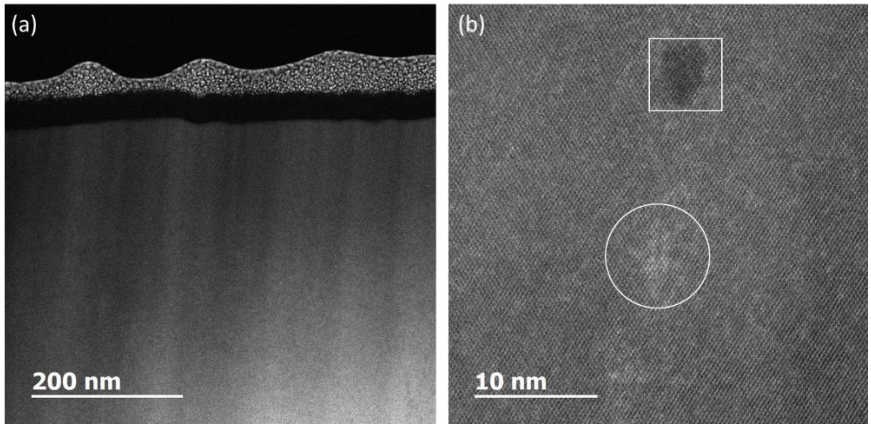

Figure 4-9: (a) HAADF TEM image of GaAsBi film grown at 325°C showing some surface roughness and intensity contrast; (b) higher magnification image of the same sample showing a Bi rich cluster (circled) and a nearby void (boxed).

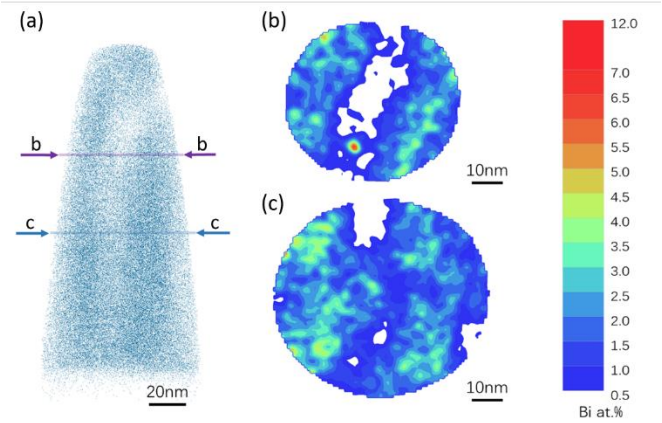

Figure 4-10: (a) APT reconstruction of the Bi distribution in the film grown at 325°C; (b) and (c) Bi isoconcentration plots of a slice along a direction of the tip from (a) showing some clusters ofup to 7 at% Bi

Reducing the growth temperature further to 315°C results in a significantly rougher surface according to the cross-sectional HAADF TEM (Fig. 4-11b), and clearer contrast variations that appear to be correlated to the surface roughening. In contrast to the sample grown at 325°C where there was only a single high Bi concentration cluster observed in the APT volume, this lower temperature sample exhibits many Bi-rich clusters that are aligned parallel to the low-Bi regions. These features are visible in both in the TEM (Fig. 4-11b) and in the APT reconstruction seen in Fig. 4-12a. The isoconcentration plots in Figs. 4-12 b-c show that the Bi concentration in the clusters reaches 12.5 atomic %, or a composition of 25%. The heavy amount of clustering is reflected in the fact that the Pearson coefficient reaches a value of 1.0. In addition to the more intense clustering, nanopores are also visible having diameters ~3 nm that penetrate from the surface down to ≤100nm, as can be seen in Figs. 4-11 a-c. Higher resolution images of the clusters (Fig. 4-11c) shows that they retain the zincblende structure. The composition modulation, clustering, and nanopores appear to have similar axes of alignment, with the angle ranging from 77 to 83 degrees relative to the surface, which corresponds to a (n11) crystal plane where n can range between 5 to 8. This relative alignment is most clear in Fig. 4-11b, which shows how voids, strings of clusters, and the lateral composition modulation are all aligned.

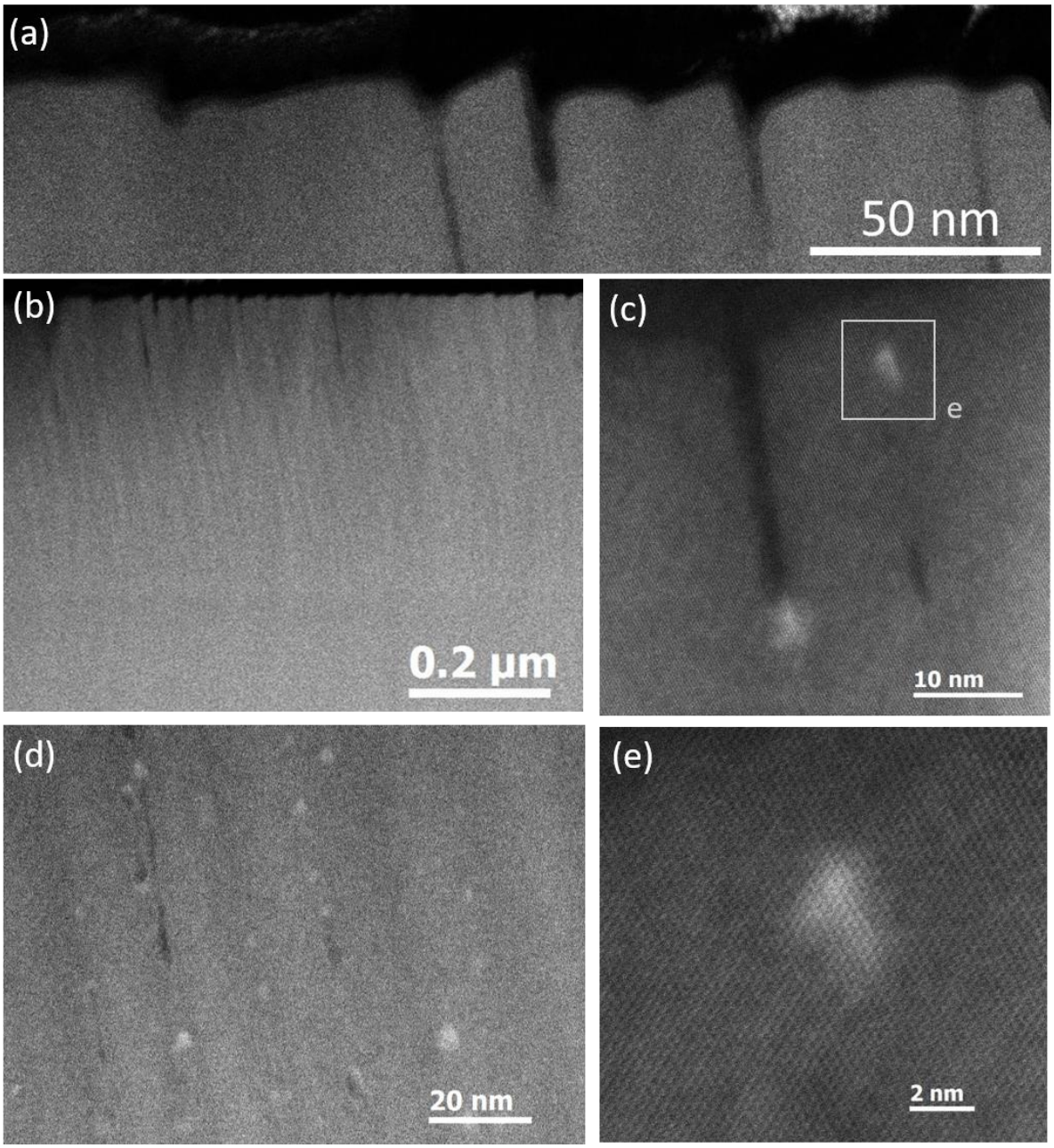

Figure 4-11: HAADF TEM images of GaAsBi film grown at 315°C. (a) image of the surface roughness and the periodic nanopores of varying depth. (b) larger scan area showing signs of lateral composition modulation and some nanopores; (c) region of interest in (b) showing a nanopore that is terminated by a Bi rich cluster as well as a cluster embedded in the film; (d) another region of interest in (b) shows many Bi rich clusters along with the composition modulation along similar axes; (e) zoom in of cluster in (c) revealing the clusters remain zincblende in structure;

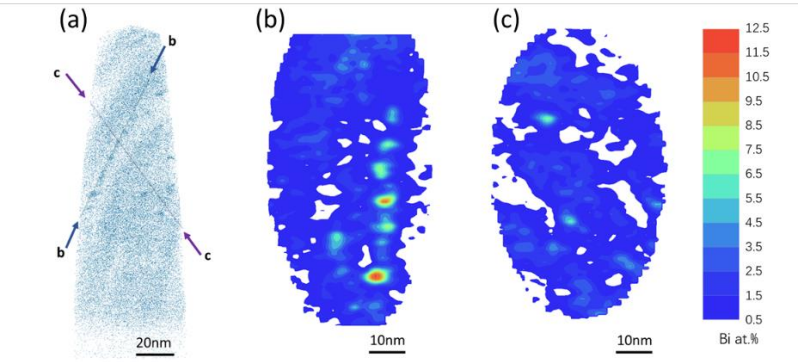

Figure 4-12: (a) APT reconstruction of the Bi distribution in the film grown at 315°C; (b) and (c) Bi isoconcentration plots of a slice along a direction of the tip from (a) showing clusters of up to 12.5 at% Bi

Lateral composition modulation and clustering have been reported separately in these alloys, but not in a single sample. A similar lateral composition modulation was observed in $GaAs_{0.985}Bi_{0.015}$ alloys by Wu et al.[18], except that those samples were grown at a much lower growth temperature (T=220°C). That modulation closely reflects the samples described here, namely the average compostion of ~1.5% and modulation period of ~25 nm. Wu et al. also report significant surface roughness correlated to the lateral composition modulation, according to the TEM images. A different report shows that annealing of $GaAs_{0.985}Bi_{0.015}$ alloys results in the appearance of Bi-rich clusters that are either zincblende for small clusters (~12nm) or rhombohedral Bi for larger clusters (~16nm), as well as the appearance of rhombohedral As clusters ~5 nm in size.[26] This is in contrast to the samples in our paper, which exhibit only zincblende Bi-rich clusters in the absence of an annealing step. Another difference between the two observed lateral composition modulations is the one discussed by Luna et al.[27] is clearly occurring along the [110] and $[1\bar{1}0]$ directions, while our modulation has a slight angle to it. This could suggest a different mechanism at play than the suface spinodal decomposition as suggested by Luna. It is also uncertain whether these are planar features or columnar like the modulations observed in Luna et al.[27]. To determine this we would either need a HAADF image

along the perpendicular axis to the images presented here or a plan view image to determine the footprint of the modulation.

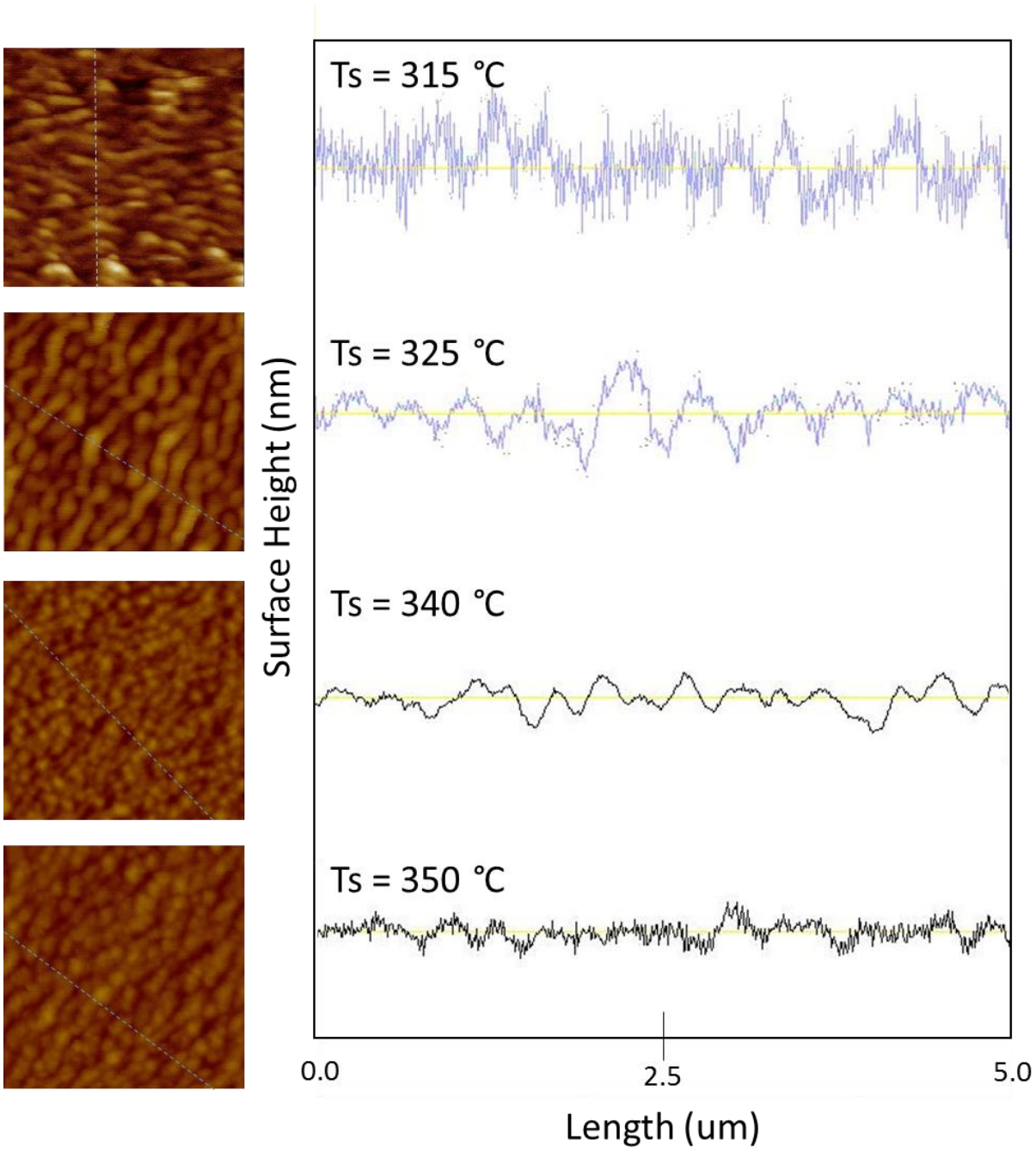

Figure 4-13: Comparison of line traces in 5 x 5 μm^2 AFM scans on the 4 samples ranging from 315-350°C. All line traces as seen on right are on the same height scale of ±9.5nm along an axis of asymmetry in the scan areas as seen on the left.

Because the lateral composition modulation, clusters, nanopores, and surface roughness appear to be aligned, it is likely that they are correlated. These experiments show that lower growth temperature lead to both rougher surfaces and a more evident composition modulation. While it is not clear whether the surface roughness drives the lateral composition modulation, or vice versa, it is likely that one provides positive feedback to the other. Figure 4-13 shows a set of linescans for 5 x 5 μm^2 showing that there appears to be a preferred direction for the surface roughening. The preferred axis would also be the assumed direction of our observed lateral composition modulation. This type of behavior has been observed in other systems. For example, growth of AlGaAs on patterned GaAs resulted in a composition modulation and lateral strain modulation with the same period as the pattern [28]. Phase separation in the bulk was observed to be correlated to the surface step structure in films of GaInAsSb [29]. The formation of the composition modulation was shown to be associated with surface corrugation in ZnSSe layers[30]. Experimental [28] and theoretical [31]investigations show that both composition modulation and surface roughness arise due to differences in surface adatom diffusion rates and relative atomic size. In fact, Spencer and Voorhees suggest that for a given atomic size mismatch (e. g. the relative size difference between Bi and As atoms), there is a critical ratio of the Bi and As diffusivity below which a growing film is unstable to morphological and compositional variations. According to this view, any changes to the relative surface diffusivity via a change in the growth temperature could induce such an instability. Spencer, Voorhess, and Tersoff [31] show that destabilization of the film will occur for a compressively strained film when the diffusivity of the larger atomic specie (Bi) slows relative to the other (As).

The TEM images and APT reconstructions show that Bi-rich clusters form in regions of reduced Bi composition along preferred directions. This implies that Bi diffuses through the

bulk along these directions. The appearance of nanopores aligned along these directions, and often terminating at Bi-rich clusters (see Fig. 4c) suggests a possible diffusion mechanism. It has been shown that GaAs films grown at low temperatures (T<320°C) contain an increasing concentration of Ga vacancies with decreasing temperature [32,33]. It has also been postulated that the addition of Bi to III-V compounds increases the vacancy concentration due Bi segregation.[34,35] It is also shown through DFT calculations that Bi incorporation may increase the Ga vacancy concentration and that the Ga vacancies can act as nucleation centers for phase separation[36]. Therefore, we hypothesize that such an increase in Ga-vacancy concentration due to these two effects enables bulk Bi diffusion and the nucleation and growth of clusters observed in the samples grown at 315C. As the Bi-diffusion process is mediated by vacancies, those vacancies may agglomerate initially into voids (as seen in Fig. 2b) and later into nanopores (as seen in Fig. 4) as the Bi atoms sweep through the volume. The expected result would be Bi-enriched clusters, vacancy-enriched clusters (the voids and nanopores), in a field of reduced Bi composition, as observed in our results.

4.5 Summary

This chapter has shown a range of inhomogeneities that exist in particular growth conditions. The first part of this chapter showed that growth in V-deficient conditions results in Ga droplet nucleation. The Ga droplets create multiple incorporation regimes for Bi on the growth surface. The result in the bulk is a wide variety of Bi composition appearing in a stripe-like pattern. The easiest path for avoidance of this type of inhomogeneity is to grow with just enough group V flux to avoid Ga droplet formation.

The latter section of this chapter shows a series of GaAsBi films with clean surfaces at a variety of growth temperatures. As the temperature decreases the surface is increasingly rough

while also exhibiting the formation lateral composition modulation, clustering, and nanopores at 315°C. The features are likely induced due to differences in the diffusivity of the constituent atoms, and by the increase in Ga-vacancies with increasing Bi composition. This suggests a potential minimum temperature required for homogeneous Bi incorporation resulting in a maximum Bi composition determined by the Bi saturation at the critical temperature.

This chapter effectively shows that homogeneous Bi incorporation in III-V-Bi films will only occur under droplet free conditions provided that the temperature is also high enough to avoid the surface roughening and lateral composition modulation discussed here. The phase space for these growth conditions has already been explored some via KMC simulations.

4.6 References

1. Rodriguez, G. V. & Millunchick, J. M. Predictive modeling of low solubility semiconductor alloys. *J. Appl. Phys.* **120,** (2016).
2. Cho, Y. H. *et al.* 'S-shaped' temperature-dependent emission shift and carrier dynamics in InGaN/GaN multiple quantum wells. *Appl. Phys. Lett.* **73,** 1370–1372 (1998).
3. Wakahara, A., Tokuda, T., Dang, X.-Z., Noda, S. & Sasaki , A. Compositional inhomogeneity and immiscibility of a GaInN ternary alloy. *Appl. Phys. Lett.* **71,** 906 (1997).
4. Ishida, K., Nomura, T., Tokunaga, H., Ohtani, H. & Nishizawa, T. Miscibility gaps in the GaPInP, GaPGaSb, InPInSn and InAsInSb systems. *J. Less-Common Met.* **155,** 193–206 (1989).
5. Berding, M. A., Sher, A., Chen, A. B. & Miller, W. E. Structural properties of bismuth-bearing semiconductor alloys. *J. Appl. Phys.* **63,** 107–115 (1988).
6. Ueda, O., Takikawa, M., Komeno, J. & Umebu, I. Atomic structure of ordered InGaP crystals grown on (001) GaAs substrates by metalorganic chemical vapor deposition. *Jpn. J. Appl. Phys* **26,** L1824 (1987).
7. Reyes, D. F. *et al.* Bismuth incorporation and the role of ordering in GaAsBi/GaAs structures. *Nanoscale Res. Lett.* **9,** 23 (2014).
8. Dorin, C., Mirecki Millunchick, J. & Wauchope, C. Intermixing and lateral composition modulation in GaAs/GaSb short period superlattices. *J. Appl. Phys.* **94,** 1667–1675 (2003).
9. Yashar, P., Pillai, M. R., Mirecki-Millunchick, J. & Barnett, S. A. X-ray diffraction measurement of segregation-induced interface broadening in InxGa1-xAs/GaAs

superlattices. *J. Appl. Phys.* **83,** 2010–2013 (1998).

10. Sakaguchi, R., Akiyama, T., Nakamura, K. & Ito, T. Theoretical investigations of compositional inhomogeneity around threading dislocations in III-nitride semiconductor alloys. *Jpn. J. Appl. Phys.* **55,** (2016).

11. Stemmann, A., Heyn, C., Köppen, T., Kipp, T. & Hansen, W. Local droplet etching of nanoholes and rings on GaAs and AlGaAs surfaces. *Appl. Phys. Lett.* **93,** 1–4 (2008).

12. Lu, X., Beaton, D. a., Lewis, R. B., Tiedje, T. & Whitwick, M. B. Effect of molecular beam epitaxy growth conditions on the Bi content of GaAs[sub 1−x]Bi[sub x]. *Appl. Phys. Lett.* **92,** 192110 (2008).

13. Lewis, R. B., Masnadi-Shirazi, M. & Tiedje, T. Growth of high Bi concentration GaAs1−xBix by molecular beam epitaxy. *Appl. Phys. Lett.* **101,** 82112 (2012).

14. Tait, C. R. & Millunchick, J. M. Kinetics of droplet formation and Bi incorporation in GaSbBi alloys. *J. Appl. Phys.* **119,** (2016).

15. Tait, C. R., Yan, L. & Millunchick, J. M. Droplet induced compositional inhomogeneities in GaAsBi. *Appl. Phys. Lett.* **111,** 1–5 (2017).

16. Janotti, a., Wei, S.-H. & Zhang, S. Theoretical study of the effects of isovalent coalloying of Bi and N in GaAs. *Phys. Rev. B* **65,** 115203 (2002).

17. Liu, X. *et al.* Native point defects in low-temperature-grown GaAs. *Appl. Phys. Lett.* **67,** 279 (1995).

18. Wu, M. *et al.* Detecting lateral composition modulation in dilute Ga(As,Bi) epilayers. *Nanotechnology* **26,** 425701 (2015).

19. Wood, A. W., Collar, K. & Li, J. Spontaneous formation of three- dimensionally ordered Bi-rich nanostructures within GaAs 1 − x Bi x / GaAs quantum wells.

20. Ptak, A. J. *et al.* Kinetically limited growth of GaAsBi by molecular-beam epitaxy. *J. Cryst. Growth* **338,** 107–110 (2012).

21. Suzuki, T. & Nishinaga, T. First real time observation of reconstruction transition associated with Ga droplet formation and annihilation during molecular beam epitaxy of GaAs. *J. Cryst. Growth* **142,** 49–60 (1994).

22. Wood, A. W., Collar, K., Li, J., Brown, A. S. & Babcock, S. E. Droplet-mediated formation of embedded GaAs nanowires in MBE GaAs $_{1-x}$ Bi $_{x}$ films. *Nanotechnology* **27,** 115704 (2016).

23. Field, R. L. *et al.* Influence of surface reconstruction on dopant incorporation and transport properties of GaAs(Bi) alloys. *Appl. Phys. Lett.* **109,** 252105 (2016).

24. Schwarz, S. M., Kempshall, B. W., Giannuzzi, L. A. & McCartney, M. R. Avoiding the curtaining effect: Backside milling by FIB INLO. *Microsc. Microanal.* **9,** 116–117 (2003).

25. Moody, M. P., Stephenson, L. T., Ceguerra, A. V. & Ringer, S. P. Quantitative binomial distribution analyses of nanoscale like-solute atom clustering and segregation in atom

probe tomography data. *Microsc. Res. Tech.* **71,** 542–550 (2008).

26. Wu, M., Luna, E., Puustinen, J., Guina, M. & Trampert, A. Formation and phase transformation of Bi-containing QD-like clusters in annealed GaAsBi. *Nanotechnology* **25,** 205605 (2014).

27. Luna, E., Wu, M., Puustinen, J., Guina, M. & Trampert, A. Spontaneous formation of nanostructures by surface spinodal decomposition in GaAs1-xBix epilayers. *J. Appl. Phys.* **117,** 185302 (2015).

28. Darowski, N., Pietsch, U., Zeimer, U., Smirnitzki, V. & Bugge, F. X-ray study of lateral strain and composition modulation in an AlGaAs overlayer induced by a GaAs lateral surface grating. *J. Appl. Phys.* **84,** 1366–1370 (1998).

29. Wang, C. A. Correlation between surface step structure and phase separation in epitaxial GaInAsSb Correlation between surface step structure and phase separation in epitaxial GaInAsSb. **2077,** 10–13 (2000).

30. Tomiya, S., Okuyama, H. & Ishibashi, A. Relation between interface morphology and recombination-enhanced defect reaction phenomena in II-VI light emitting devices. *Appl. Surf. Sci.* **159,** 243–249 (2000).

31. Spencer, B. J., Voorhees, P. W. & Tersoff, J. Stabilization of strained alloy film growth by a difference in atomic mobilities Stabilization of strained alloy film growth by a difference in atomic mobilities. *Appl. Phys. Lett.* **76,** 3022 (2000).

32. Gebauer, J. *et al.* Ga vacancies in low-temperature-grown GaAs identified by slow positrons. *Appl. Phys. Lett.* **71,** 638–640 (1997).

33. Liu, X. *et al.* Native point defects in low-temperature-grown GaAs. *Appl. Phys. Lett.* **67,** 279 (1995).

34. Wang, S., Song, Y. & Roy, I. S. Bismuth incorporation and lattice contraction in GaSbBi and InSbBi. *2011 13th Int. Conf. Transparent Opt. Networks* **3,** 1–3 (2011).

35. Song, Y., Wang, S., Saha Roy, I., Shi, P. & Hallen, A. Growth of GaSb1−xBix by molecular beam epitaxy. *J. Vac. Sci. Technol. B Microelectron. Nanom. Struct.* **30,** 02B114 (2012).

36. Punkkinen, M. P. J. *et al.* Does Bi form clusters in GaAsBi alloys? *Semicond. Sci. Technol.* **29,** 115007 (2014).

37. Yan, Lifan. Compositional Inhomogeneity and Defects in Nanomaterials for Optoelectronics (2017)

Chapter 5: Optimizing Growth and Future Directions

5.1 Directing future growths

Over the course of this dissertation it was shown that the existence of droplets on the surface of these III-V-Bi alloys is indicative of the films being inhomogeneous in Bi composition. It was also learned that even with a clean surface if the growth temperature is not high enough the surface can roughen and result in a variety of inhomogeneities, such as lateral composition modulation, clustering, and nanopores. This generates two possible paths forward for material development. One direction is determining what compositions are experimentally accessible with clean surfaces and a sufficient growth temperature for smooth surfaces. The other direction is to grow films in the undesirable regimes and find methods to mitigate the inhomogeneities that appear.

5.2 Determining the growth parameters for clean smooth surface films

Now that it is understood what impact droplets have on the surface, instead of looking at every possible film to determine its composition and behavior we can instead map out the growth parameters that have higher potential for quality films. The temperature series in an earlier section suggests that 325°C would be a reasonable threshold temperature for avoiding the surface roughening and lateral composition modulation phenomena. SEM and EDS will be sufficient characterization for these films since it only needs to be known if droplets exist on the surface.

5.3 Mitigating Inhomogeneities

With such a small parameter space available for clean and smooth surface films is limiting to accessible Bi compositions and the ability to grow these materials on any given system. To improve the window available ways to diminish or remove the inhomogeneities that appear in the problematic regimes such as too low of temperature or droplet formation need to be found.

5.3.1 Growth interrupts

The proposed mechanic for the inhomogeneity caused by Ga droplets is the variety of available Ga flux across the surface. Interrupting the growths by letting the film periodically anneal under an As flux resulted in a significantly more homogeneous Bi distribution than without the interrupts. The enhanced Bi incorporation in the interrupted film still appears over somewhat regular intervals corresponding to the interruption frequency.

The significant improvement to the homogeneity of the film generated by the growth makes growth interrupts a promising avenue for homogenous growth in conditions that normally results in Ga droplets on the surface. There are a few directions for optimization including interruption frequency and duration. The upper limit for interruption frequency of monolayer growth may not be the best option as it is possible Bi would not be able to incorporate and be trapped in the metastable state in the bulk crystal. If most of the enhanced Bi incorporation is occurring at the restart of growth then longer interruptions under As would aid in consumption of the excess Ga.

5.3.2 GaAsBi/GaAs superlattice

Superlattices are another approach that could yield significant improvement for homogeneity. This is a similar approach to the growth interrupts except instead of temporary annealing under As, an intermediary layer of GaAs is grown. There is an example of these superlattices

illustrating good interfaces and uniform Bi distribution[1]. Since the GaAs layer in the superlattice can be grown under group V rich conditions, doing so would perform similar removal of excess Ga buildup. This could allow growth in Ga droplet formation conditions for maximal Bi incorporation while mitigating the inhomogeneity due to Ga droplets.

Superlattices will also provide insight into how accurately layers are deposited. The XRD traces will have characteristic satellite peaks where the separation is determined by the thickness of the repeating layer. A few preliminary samples have been grown targeting 10 repeated layers of GaAsBi/GaAs with thicknesses of 50nm/25nm and 50nm/12.5nm at 325°C. The fluxes match the conditions for the 500nm layer of GaAsBi grown at 325°C with conditions found in table 4-1. The composition of the GaAsBi layers in the superlattice are assumed to match this sample at 2.2%.

Figure 5-1 shows a comparison of the 004 rocking curve data for the 2 superlattices to a simulated fit using the estimated composition and targeted thickness listed above. The simulated satellite peak separation is smaller than the actual data for both samples. This means that the thicknesses are not what was targeted in the initial growth. A better fit for the superlattices is shown in Fig. 5-2, where the thicknesses are 42nm/25nm and 39nm/15nm. The significant reduction in GaAsBi thickness could be a result of the growth conditions being group V limited linking the growth rate to the group V flux instead of the Ga flux. The well-defined satellites suggest that the interfaces are well defined as found in other work[1].

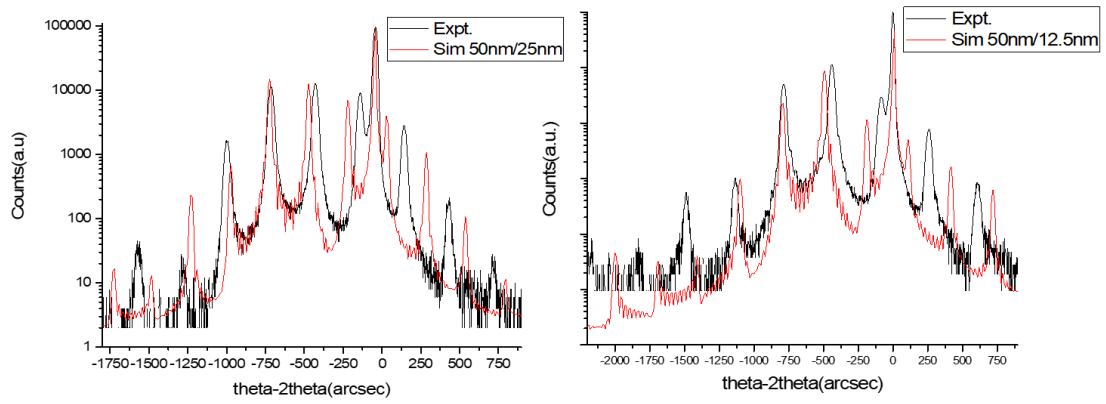

Figure 5-1: Experimental vs. Simulated XRD using targeted superlattice thicknesses

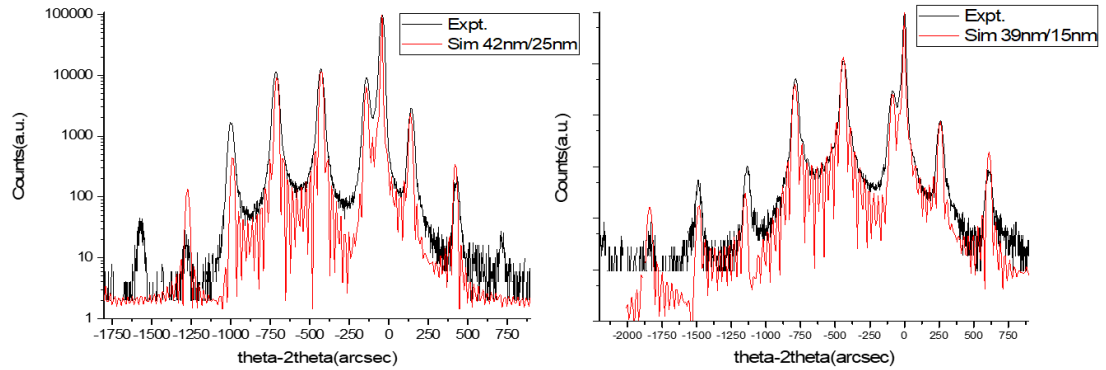

Figure 5-2: Experimental vs. Simulated XRD using superlattice thicknesses for best fit

Future directions for the superlattices are plentiful. Since it is an extension of the growth interrupts superlattices, they could be attempted with a variety of thicknesses where the GaAsBi layer is grown under increasing group V deficient conditions. The satellite peak definition would be an initial guide for the homogeneity similar in fashion to section 4.3. In addition to potential improvement in the Ga droplet regime, superlattices could improve the surface roughening induced inhomogeneities. This hypothesis depends on whether the GaAs layer helps reduce the surface roughness at a given temperature. This follows based on the proposed mechanism of the growth destabilization discussed in section 4.4.

5.4 Extension to GaSbBi

Recently there has been success in the synthesis and characterization of high Bi GaSbBi films[2–4]. The projects within this dissertation began with mostly experiments in GaSbBi and transitioned into GaAsBi. An interesting extension of this work is to examine if the inhomogeneity phenomena observed in GaAsBi discussed in chapter 4 behaves similarly in GaSbBi. If the proposed mechanisms for the inhomogeneities are true there should be inhomogeneity found with Ga droplets but less likely with reduced temperature. This is because the temperature boundary is a dynamic between the size and diffusion differences of Bi vs. As or Sb. The size difference is smaller and the diffusion relationship would be different. Observation of these dynamics would be more difficult in HAADF TEM imaging because Sb is closer in mass to Bi resulting in much lower contrast. Determination of homogeneity will be more reliant on APT and potentially EDS if the composition range is suitable.

5.5 Investigation of Strain on Bi Incorporation

A final direction for the project is to determine how strain affects incorporation of Bi. It's possible for strain energy to be contributing to the inohomogeneities that are observed and discussed in this dissertation. Since the range of observed inhomogeneities is greater in GaAsBi and easier to detect, it is the most sensible starting point. A range of substrate lattice parameter would be accessed through metamorphic buffer layers of either InGaAs or GaAsSb[5]. An increase in the substrate lattice parameter will increase the solubility of Bi in GaAs and will alter the strain energy of the system.

An easier system to investigate in this regard would be InAsBi due to GaSb being close in lattice parameter size to InAs as a substrate. The dynamics in this system will be easier to manipulate since the substrates would not depend on creating them experimentally before use.

5.6 References

1. Chen, W. *et al.* Atom probe tomography evidence for uniform incorporation of Bi across the growth front in GaAs1-xBix/GaAs superlattice. *J. Cryst. Growth* **446,** 27–32 (2016).

2. Luna, E. *et al.* Microstructure and interface analysis of emerging Ga(Sb,Bi) epilayers and Ga(Sb,Bi)/GaSb quantum wells for optoelectronic applications. *Appl. Phys. Lett.* **112,** 151905 (2018).

3. Yue, L. *et al.* Structural and optical properties of GaSbBi/GaSb quantum wells [Invited]. *Opt. Mater. Express* **8,** 893 (2018).

4. Rajpalke, M. K. *et al.* High Bi content GaSbBi alloys. *J. Appl. Phys.* **116,** 043511 (2014).

5. Liu, H. Y., Qiu, Y., Jin, C. Y., Walther, T. & Cullis, A. G. 1.55 μm InAs quantum dots grown on a GaAs substrate using a GaAsSb metamorphic buffer layer. *Appl. Phys. Lett.* **92,** (2008).